IDENTIFICATION OF SIGNALLING FACTORS DETERMINING RESISTANCE TO ALPELISIB (BYL-719)-FULVESTRANT MEDIATED GROWTH INHIBITION IN PIK3CA MUTANT BREAST CANCERS

A THESIS SUBMITTED TO
THE GRADUATE SCHOOL OF ENGINEERING AND SCIENCE
OF BILKENT UNIVERSITY
IN PARTIAL FULFILLMENT OF THE REQUIREMENTS FOR
THE DEGREE OF MASTER OF SCIENCE
IN
MOLECULAR BIOLOGY AND GENETICS

By

Esra Selin Emirmustafaoğlu

August 2024

IDENTIFICATION OF SIGNALLING FACTORS DETERMINING RESISTANCE TO ALPELISIB (BYL-719)-FULVESTRANT MEDIATED GROWTH INHIBITION IN PIK3CA MUTANT BREAST CANCERS

By Esra Selin Emirmustafaoğlu

August 2024

We certify that we have read this thesis and that, in our opinion, it is fully adequate, in scope and in quality, as a thesis for the degree of Master of Science.

Onur Çizmecioğlu (Advisor)

Işık Yuluğ

Sreeparna Banerjee

Approved for the Graduate School of Engineering and Science:

Orhan Arıkan

Director of the Graduate School

ACKNOWLEDGEMENTS

I would like to express my deepest gratitude to my supervisor, Dr. Onur Çizmecioğlu, for his invaluable guidance, support, and mentorship throughout my research journey. His insights and encouragement have been instrumental in the completion of this thesis. I would also like to extend my thanks to my colleagues for their collaboration, assistance, and the stimulating discussions that helped shape this work.

My appreciation goes to the Bilkent University Molecular Biology and Genetics Department for providing the facilities and resources necessary for this research. Special thanks to Prof. Dr. Özgür Şahin for his mentorship and assistance, which greatly contributed to the project's progress.

I am deeply grateful to my family, whose unwavering support and encouragement have been the foundation of my journey. To my parents, thank you for believing in me and for your endless love, guidance, and sacrifices, which have made all of this possible. To my sister and brother-in-law, your constant support and reassurance have been a source of strength throughout this process. To my nephew, your joy and laughter have provided me with the much-needed motivation to persevere. To my boyfriend, thank you for your unwavering love, patience, and encouragement. I am truly blessed to have such a wonderful support system, and I dedicate this achievement to all of you.

Lastly, I would like to thank TUBITAK for granting me the BIDEB 2210A National M.Sc. Scholarship and funding this project (Project no: 1001-120Z634).

Table of Contents

LIST OF FIGURES

LIST OF TABLES

ABBREVIATIONS

PI3K	**Phosphatidylinositol-3 kinase**
PIP3	**Phosphatidylinositol-3,4,5-triphosphate**
PIP2	**Phosphatidylinositol-4,5-bisphosphate**
AKT	**Protein Kinase B**
PTEN	**Phosphatase and tensin homolog**
mTOR	**Mammalian target of rapamycin**
RTK	**Receptor tyrosine kinase**
GPCR	**G-Protein coupled receptor**
PDGF	**Platelet-derived growth factor**
FGFR	**Fibroblast Growth Factor Receptor**
MAPK	**Mitogen Activated Protein Kinase**
SRB	**Sulforhodamine B**
BYLR	**Alpelisib (BYL-719) resistant**
FulvR	**Fulvestrant resistant**
FDA	**U.S Food and Drug Administration**
TamR	**Tamoxifen resistant**
DEGs	**Differentially expressed genes**
PtdIns	**Phosphoinositides**

ABSTRACT

IDENTIFICATION OF SIGNALLING FACTORS DETERMINING RESISTANCE TO ALPELISIB (BYL-719)-FULVESTRANT MEDIATED GROWTH INHIBITION IN PIK3CA MUTANT BREAST CANCERS

Esra Selin Emirmustafaoğlu

M.S. in Molecular Biology and Genetics

Advisor: Onur Çizmecioğlu

August, 2024

Luminal A breast cancer, characterised by hormone receptor positivity and human epidermal growth factor receptor 2 negativity, represents approximately 70% of all reported cases of breast cancer. Mutations in components of the PI3K pathway, particularly p110α and PTEN, are commonly observed subsequent to p53 mutations in these cancers. Consequently, PI3K inhibitors are employed to treat breast tumours characterised by PI3KCA mutations. Nevertheless, inhibiting the PI3K pathway may give rise to the activation of other signalling pathways, hence inducing the development of drug resistance. The objective of this study is to examine the potential activation of pathways associated with the FDA-approved combined use of Alpelisib (BYL-719) and Fulvestrant in the treatment of PIK3CA mutant breast cancer. In this study, MCF7 and T47D cell lines developed acquired resistance to the Alpelisib/Fulvestrant combination. The resistant cells were then subjected to comparative

transcriptome analysis to identify putative resistance networks. Our results implicate various components of the MAPK pathway as a potential resistance factor in both cellular models. We also corroborated these results via immunoblot analysis of the respective signalling cascades. Therefore, we assessed the potency of the combination of Pemigatinib, an FGFR inhibitor and alpelisib and have shown that this combination is successful in inhibiting the growth of the resistant cell lines. We also supported our findings by performing 3D growth assays with this combination. The findings of our study will contribute to the advancement of therapeutic strategies for luminal A breast cancer, particularly in the context of Alpelisib/Fulvestrant drug resistance.

ÖZET

PIK3CA MUTANT MEME KANSERLERİNDE ALPELİSİB (BYL-719)-FULVESTRANT ARACILI BÜYÜME ENGELLEMESİNE DİRENÇ OLUŞTURABİLECEK SİNYAL AĞI ETKİNLİKLERİNİN BELİRLENMESİ

Esra Selin Emirmustafaoğlu

Moleküler Biyoloji ve Genetik, Yüksek Lisans

Tez Danışmanı: Onur Çizmecioğlu

Ağustos, 2024

Luminal A meme kanseri, hormon reseptör pozitifliği ve insan epidermal büyüme faktörü reseptör 2 negatifliği ile karakterize edilen ve tüm meme kanseri vakalarının yaklaşık %70'ini oluşturan bir alt tiptir. Bu kanserlerde p53 mutasyonlarından sonra PI3K yolunun bileşenlerinde, özellikle p110alpha ve PTEN'de mutasyonlar sıkça gözlemlenir. Bu nedenle PI3KCA mutasyonları ile karakterize edilen meme kanseri tümörlerinin tedavisinde PI3K yolağı inhibitörleri kullanılmaktadır. Bununla birlikte, PI3K yolağının inhibisyonu, diğer sinyal yolağlarının aktivasyonuna yol açabilir ve bu da ilaç direncinin gelişimine sebep olabilir. Bu çalışmanın amacı, PIK3CA mutant meme kanserlerinin tedavisinde Alpelisib (BYL-719) ve Fulvestrant'ın FDA onaylı kombine kullanımına bağlı olarak direnç gelişimi ile potensiyel olarak aktifleşebilecek yolağlarını incelemektir. Bu çalışmada, MCF7 ve T47D hücre hatları Alpelisib-Fulvestrant kombinasyonuna karşı direnç geliştirmiştir.

Dirençli hücreler, olası direnç mekanizmalarını belirlemek amacıyla karşılaştırmalı transkriptom analizine tabi tutulmuştur. Sonuçlarımız, her iki hücre modelinde de MAPK yolağının çeşitli bileşenlerinin potansiyel bir direnç faktörü olarak rol oynayabileceğini işaret etmektedir. Bu sonuçları ilgili sinyal yolağlarının immünoblot analizi ile de doğruladık. Bu nedenle, Pemigatinib ve alpelisib kombinasyonunun etkinliğini değerlendirdik ve bu kombinasyonun dirençli hücre hatlarının büyümesini engellemede başarılı olduğunu gösterdik. Bulgularımızı, bu kombinasyon ile üç boyutlu hücre büyüme analizleri yaparak da destekledik. Çalışmamızın bulguları, özellikle Alpelisib/Fulvestrant ilaç direnci bağlamında, Luminal A meme kanserine yönelik terapötik stratejilerin ilerlemesine katkıda bulunacaktır.

1. INTRODUCTION

1.1 Background and Significance

1.1.1 Overview of Breast Cancer

Breast cancer is the most diagnosed cancer type and accounts for 15.5% of the new cancer cases in the United States. It is the second most prevalent cause of death among women worldwide (Siegel et al., 2024). Breast cancer might occur at any age after puberty; however, the incidence rate increases with age. The incidence rate is also higher in more developed countries compared to the countries with low Human Development Index (HDI). This is attributed to the differences in lifestyle, reproductive factors and opportunity to access screening and diagnostic services.

The strongest risk factor for breast cancer is female gender; 99% of the cases are female, whereas 0.5-1% of the cases are male. Ageing, alcohol abuse, obesity, BC history in the family, post-menopausal hormone therapy and tobacco use are among the factors which increase the risk of breast cancer. However, almost half of the BC is diagnosed in women who have no risk factors other than being female (World Health Organization, 2024). Genetic background also constitutes a risk factor for breast cancer; certain inherited mutated genes increase breast cancer risk, such as BRCA1, BRCA2 and PALB-2 mutations.

Breast cancer is a heterogeneous disease at the molecular level, and its subtypes are determined according to the molecular characteristics of the cancer. The activation of human epidermal growth factor receptor 2 (HER2, encoded by ERBB2), the activation of hormone receptors (ER and PR), and

the mutations of BRCA are among the molecular features. According to the different expressions of hormone receptors and HER2 receptors, breast cancer is classified into four different subtypes: luminal A (HR+/HER2-), luminal B (HR+/HER2+), basal-like and triple-negative (HR-/HER2-) (Harbeck et al., 2019). Luminal-A breast cancer is the most prevalent subtype and accounts for 50%-60% of all breast cancers (Yersal et al., 2014).

1.1.2 Importance of Targeted Therapy in Breast Cancer

Targeted drug therapy involves administering medications that specifically target proteins, which promote their growth, metastasis, and prolonged survival of breast cancer cells. Targeted drugs can act to kill the cancer cells or decrease their growth rate. When compared to conventional therapies such as chemotherapy, hormone therapy and radiotherapy, targeted drugs generally have milder adverse effects (National Breast Cancer Foundation, 2024)

These drugs are given into the bloodstream and, therefore, can reach almost all parts of the body. Thus, they are also effective against cancers spread in remote areas of the body. Targeted drugs may even be successful in cases where chemotherapy is not. Moreover, some of these drugs, such as monoclonal antibodies, can help boost the immune system, and some targeted drugs may increase the effectiveness of other treatments. Targeted drugs in Luminal-A BC include CDK4/6 inhibitors, mTOR inhibitors, PI3K inhibitors, AKT inhibitors, and antibody-drug conjugates (Masoud et al).

1.2 PIK3CA Mutations in Breast Cancers

1.2.1 Phosphoinositide Kinases

Phosphoinositide kinases (PIKs) are lipid kinases that act as signal transducers within the cells, and they phosphorylate the inositol ring of phosphoinositides. PIKs are classified into three families based on the phosphorylation site of the carbohydrate: phosphoinositide 3-kinases (PI3Ks), phosphoinositide 4-kinases (PIP4Ks) and phosphoinositide 5-kinases (PIP5Ks).

Depending on the subunit structures, regulation and substrate activity, PI3Ks are also categorised into three groups: Class I, Class II and Class III. Class I PI3Ks include Class IA and Class IB, and the Class IA subgroup comprises three catalytic subunits: p110, p110, and p110γ. These catalytic subunits form heterodimers with one of five regulatory subunits of PI3K, which are p85α, p85β, p85γ, p50α, and p55α.

Activation of PI3Ks is mediated by cell surface receptor tyrosine kinases. The formation of PtdIns (3,4,5)P_3 (PIP3) is catalysed by PI3K IA and IB class enzymes. This process is reversed by the prime antagonist of PI3K, lipid phosphatase PTEN. PIP3 is an anchor for the proteins with Pleckstrin Homology (PH) domain, such as serine/threonine kinases AKT1, AKT2 and AKT3. When AKTs are located in the membrane, they get activated by 3-phosphoinositide-dependent protein kinase-1 (PDK1). AKT targets include mTOR, Caspase 9, GSKβ, Bad, Tuberin and a subset of FOX proteins. AKT activation may lead to various biological consequences, such as changes in cell proliferation, survival and motility (Samuels et al., 2010).

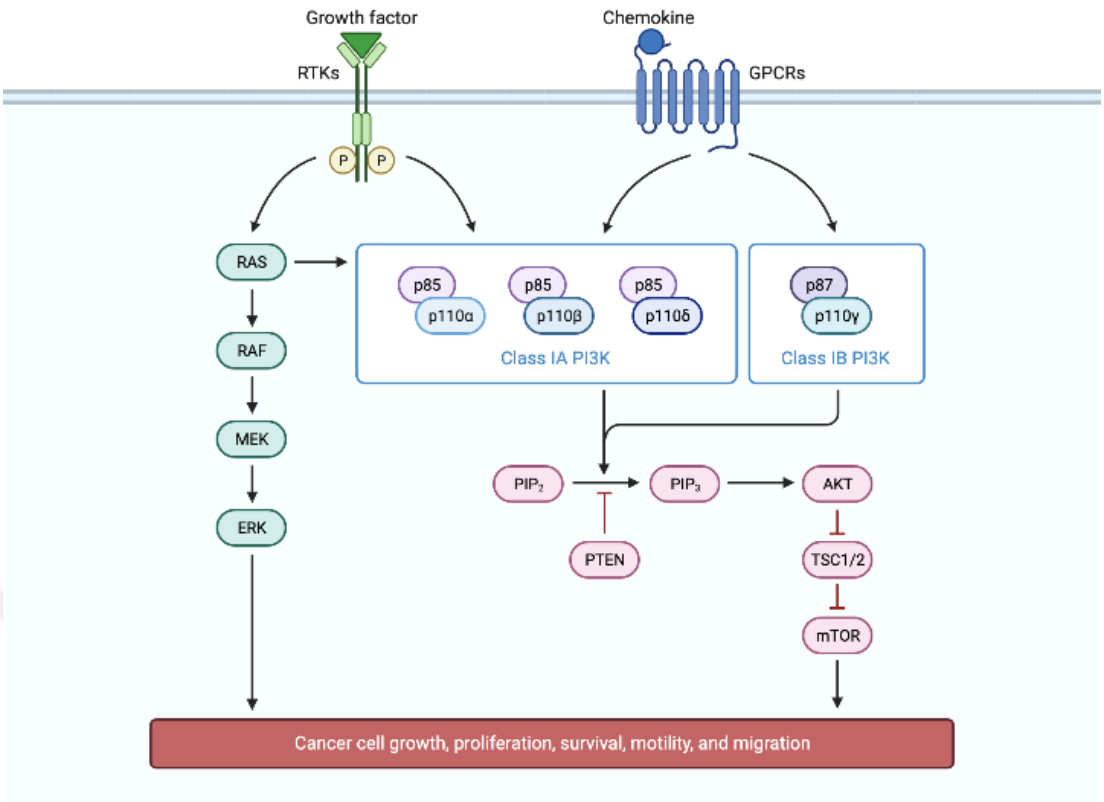

Figure 1.2.1 PI3K/Akt pathway PI3K pathway is activated upon ligand binding to receptor tyrosine kinases; it can also be activated via G-protein coupled receptors. Image was generated with BioRender.

1.2.2 Role of PIK3CA Mutations in Cancer

Alterations in the genes which regulate cell growth and differentiation lead to cancer by causing abnormal cell proliferation. The genes related to the cancer are categorised into two major classes: tumour suppressor genes and oncogenes. Under normal conditions, tumour suppressor genes inhibit cell growth; however, these become inactivated in cancer. On the other hand, oncogenes usually promote cell proliferation and growth. These oncogenes, such as protein kinases, become hyperactivated in cancer disease (Bader et al).

Dysregulation of the PI3K pathway is frequently seen in human cancers. The most prevalent genetic alterations in this pathway are the following: PTEN loss of function mutation, amplification of genomic regions where Akt is located and point mutations, which lead to the activation of PI3K. Studies have shown that PI3K pathway-related genes are frequently mutated in cancers; PIK3CA is among these most frequently mutated genes. PIK3CA encodes for the catalytic subunit of PI3K, p110α. This gene is located on chromosome 3q26.3, consists of 20 exons, and codes for a protein composed of 1068 amino acids.

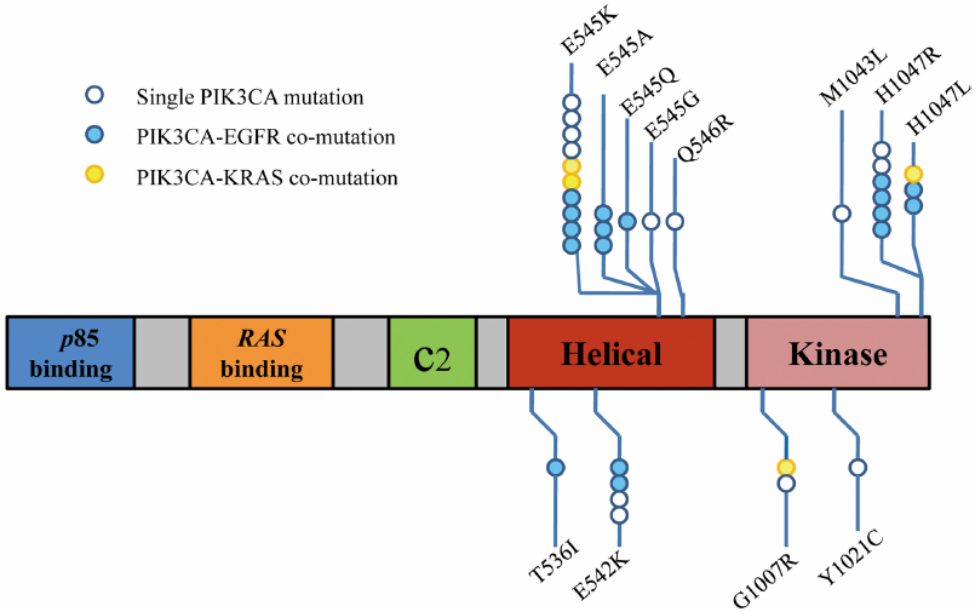

Figure 1.2.2 Mutations on PIK3CA gene The coloured boxes represent the different functional domains of the protein (p85 binding, ras binding, c2, helical and kinase). The dots coming out of the boxes represent the frequency of different type of mutations.

1.2.3 Prevalence and Impact of PIK3CA Mutations in Breast Cancer

PI3K mutations are identified in various cancer types, including colorectal, breast, ovary, brain, liver and lung (Ligresti et al., 2009). Strikingly, 40% of the primary breast cancer tumours and 28%-46% of the Luminal-A breast cancers include PIK3CA mutations (André, F et al, 2021). The most frequent mutation of the PIK3CA gene is found at the coding sequence, and it leads to a gain of function of PI3K. Three hotspot non-synonymous variants account for 87% of the clinically significant PIK3CA mutations. These mutations result in specific amino acid substitutions: COSMIC 760 in exon 9 (17% incidence) causes an E545K substitution, COSMIC 763 in exon 19 (17% incidence) affects the E545 residue, and COSMIC 775 in exon 20 (35% incidence) leads to an H1047R substitution.

These three genomic alterations determine success in drug responsiveness. Namely, diagnostic testing of the tumours can identify the patients who might benefit from PI3K-targeted therapy. FDA and EMA have recently approved the use of Alpelisib (BYL-719), a p110α inhibitor, combined with Fulvestrant for Luminal-A breast cancer patients (Reinhardt et al., 2022) (Narayan et al., 2020).

1.3 Mechanism of Action of Alpelisib and Fulvestrant

1.3.1 Overview of Alpelisib

Alpelisib (BYL-719) is a drug which is used in targeted therapy. It targets both wild-type PI3K-α and PI3K-α containing canonical mutations. Namely, it inhibits the catalytic subunit, p110α, yet it is not very potent

against the other PI3K isoforms, p110β and p110γ. alpelisib slow down the growth and proliferation of the cancer cells by inhibiting p110α (Galstyan et al. 89-105). Alpelisib is used in combination with Fulvestrant for the treatment of postmenopausal women and men with Luminal-A breast cancer, which harbours PIK3CA mutations (Narayan et al., 2020). It was approved by the FDA in 2019 and is the first PIK3CA inhibitor used for the treatment of HR-positive HER2-negative PIK3CA mutated in either advanced or metastatic breast cancers in female and male patients. (National Center for Biotechnology Information)

1.3.2 Overview of Fulvestrant

Fulvestrant is a selective estrogen receptor degrader (SERD) which binds to the estrogen receptor (ER), blocking its activity and leading to its degradation. The ER is activated by dimerisation of the receptor; when fulvestrant binds to the monomers of the receptor, it prevents these receptors from dimerising. This blocks ER activation, subsequently inhibiting its ability to regulate gene expression. Fulvestrant also inactivates the AF1 and AF2 domains of the ER, which are responsible for activating target genes. Additionally, the binding of fulvestrant to the ER reduces the receptor's ability to translocate to the nucleus and accelerates its degradation. Thus, fulvestrant effectively inhibits oestrogen signalling through the ER, preventing the promotion of cancer cell growth and proliferation (Nathan et al., 2017), (Carlson et al., 2005).

1.4 Resistance to Cancer Therapies

1.4.1 General Mechanisms of Resistance in Cancer

Drug resistance is a major challenge in cancer therapy. Resistance can already exist before taking treatments, or it can develop as a result of the treatment. There are numerous mechanisms which enable cancer cells to escape therapy. The alteration of drug transport, enhanced drug metabolism, mutation of drug targets and genetic alteration, which prevent apoptosis, are among these different mechanisms. Additionally, tumour cells are heterogeneous with respect to genetic alterations. Therefore, some cells that have acquired or harboured resistance traits might experience selective pressure during a specific treatment. Thereby, these cells can proliferate and grow despite the therapy. Multidrug resistance (MDR) generally develops due to diverse resistance mechanisms, posing significant challenges for clinical outcomes.

The development of therapeutic resistance, whether primary or acquired, decreases the efficacy and the success of the treatment for many patients. Patient survival rates significantly decrease when resistance develops against the therapy.

Understanding the genetic and biochemical background of resistance mechanisms is crucial to combating drug resistance and allowing the development of new therapies. There are distinct strategies like targeting specific oncogenes and exploiting synthetic lethality pathways in order to overcome setbacks of drug resistance. Moreover, studying the role of tumour microenvironment and tumour heterogeneity in promoting resistance might

serve to design more potent treatment approaches. The persistent challenge of drug resistance in cancer treatment is tried to be overcome by elucidating these complexities (Zahreddine and Borden).

1.4.2 Specific Resistance Mechanisms to Alpelisib

Following PI3K/AKT inhibition by alpelisib, AKT signalling is downregulated, and as a result, FOXO transcription factors translocate into the nucleus. Here, they enhance the activity of MAPK and PI3K signalling, which results in the upregulation of receptor tyrosine kinases such as HER2 and HER3. Thereby, the inhibition of the PI3K pathway is bypassed by the compensatory upregulation of RTKs, and despite the presence of alpelisib, proliferative signals are sustained within the cells (Bosch et al., 2015).

An epigenetic change occurs in ER+ breast cancers after the inhibition of AKT. Specifically, the methyl-transferase activity of KMT2D is restored, and this enzyme enhances the recruitment of transcription factors FOXA1, PBX1 and ER to ER binding sites. Thus, ER-dependent gene transcription is amplified, resulting in the promotion of cell proliferation and survival (Toska et al., 2017).

An alternative pathway is activated where serum and glucocorticoid-regulated kinase 3 (SGK3) is involved in resistance against alpelisib in the tumours harbouring PIK3CA mutations, which inherently have low levels of phosphorylated AKT. The sensitivity of the tumours to alpelisib is diminished by the activation of SGK3 and its downstream signalling pathways, specifically mTOR (Toska et al., 2019).

Another resistance mechanism involves the activation of compensatory feedback loops, which take place upon PI3K inhibition. Inhibition of 4E-BP1 phosphorylation by mTOR leads to the downregulation of PTEN, resulting in a rebound activation of AKT phosphorylation. This negative feedback loop illustrates the dynamic nature of signalling networks and the challenges associated with achieving sustained PI3K inhibition (Wright et al., 2021).

Lastly, PI3K signalling can be through different isoforms depending on the genetic background of the cells. Selective inhibition of a specific PI3K isoform, where it predominantly activates the signalling, may lead to the reciprocal activation of the other isoforms. Thereby, AKT/mTOR signalling is reactivated by the activation of the other isoforms (Wright et al., 2021).

1.5 FGF/FGFR and MAPK Signalling

1.5.1 FGF/FGFR Pathway

FGFs are a large family of growth factors categorised as paracrine, autocrine and endocrine-based on their mechanisms of action. FGFRs are a family of receptor tyrosine kinases (RTKs), and they are encoded by four genes: FGFR1, FGFR2, FGFR3 and FGFR4. FGFRs consist of three main domains: an extracellular ligand binding domain, a single-pass transmembrane domain and an intracellular tyrosine kinase domain (Xie et al).

The receptors are dimerised upon binding of FGFs and undergo autophosphorylation on tyrosine residues. This creates docking sites for

downstream signalling proteins. FGFRs activate Ras-MAPK, PI3K/Akt, PLCγ and STAT pathways, which play different roles in mediating cellular responses to FGF stimulation (Goetz et al)

1.5.2 MAPK Signalling Pathway

The Mitogen-Activated Protein Kinase (MAPK) signalling cascade plays a critical role in regulating cell growth, proliferation, differentiation and survival. MAPK pathway consists of various protein kinases that transduce signals from cell surface receptors to DNA in the nucleus, affecting gene expression processes (Zhang et al.).

ERK1/2 pathway is the most studied sub-pathway of the MAPK pathway and is often referred to as the MAPK pathway. Following the activation of receptor tyrosine kinases (RTKs) on the cell surface upon dimerisation, the receptor is autophosphorylated and recruits and activates RAS, a small GTPase. Activated RAS stimulates Raf, which is a serine/threonine kinase that leads to the activation of MEK (MAPK/ERK kinase). Then, MEK phosphorylates and activates extracellular signal-regulated kinase (ERK). ERK is translocated into the nucleus as a result of phosphorylation and activation, which leads to the regulation of several transcription factors (Zhang et al. Cargnello et al.).

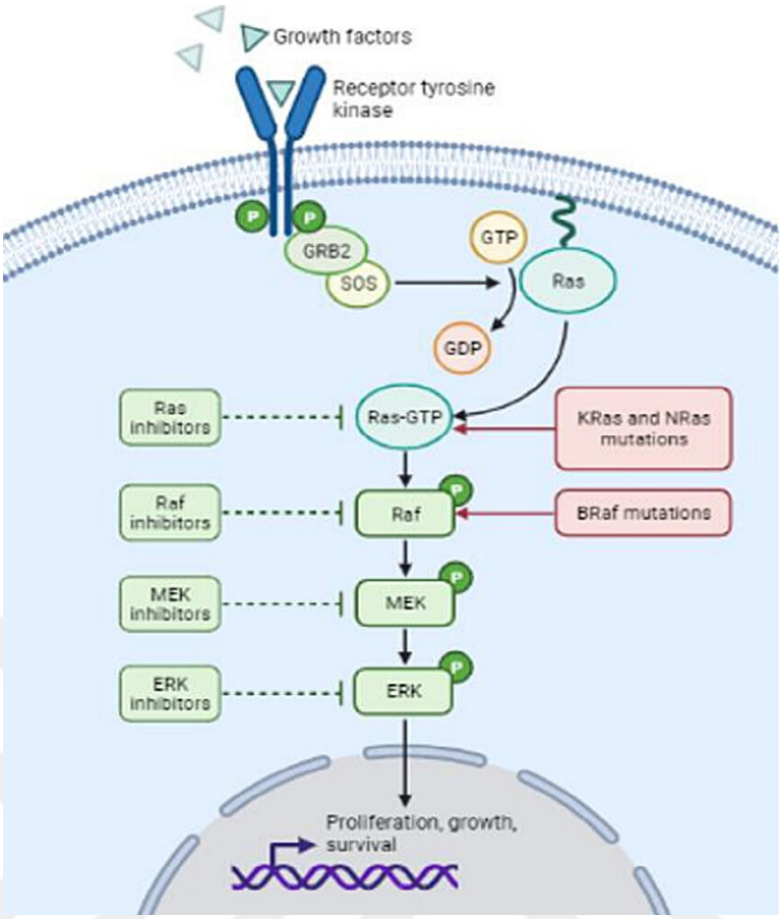

Figure 1.5.1 Schematic Representation of MAPK Pathway MAPK pathway is activated via ligand binding to receptor tyrosine kinases. Through the activation of the cascade many signalling events such as cell growth proliferation and survival can be activated. The image is generated with BioRender.

1.5.3 MAPK Signalling in Breast Cancer

The MAPK pathway involving ERK1 and ERK2 is most related to breast cancer. The major regulators of ERK1 and ERK2 are peptide growth factors which act through RTKs. MAP kinase can be activated through oestradiol, progesterone and testosterone by binding to the receptors on the cell membrane. Moreover, other molecules that bind to G-protein coupled receptors can also similarly activate MAP kinase. Studies showed a

significant proportion of cells with activated MAP kinase in breast tumours (Braicu et al.). MAP kinase pathway may affect ER-induced transcription by crosstalking in ER+ breast cancers. Estradiol activates cell proliferation via MAP kinase-involved mechanisms, increasing the growth factor production and consequently resulting in MAP kinase upregulation. The treatments used in hormone-positive breast cancers may lead to the upregulation of MAP kinase activation. *In vitro* and *in vivo* breast cancer studies showed that estradiol deprivation results in the upregulation of MAP kinase (Santen et al., 2002)

1.5.2 Interaction of MAPK Pathway with PI3K Pathway

PI3K/Akt and Ras/ERK pathways may negatively regulate the activity of each other. For instance, EGF-induced AKT activation is enhanced by the MEK inhibitors. EGF-induced ERK phosphorylation of GAB1 might be involved in this process. PI3K is recruited to the EGF receptor (EGFR) by GAB1 mediation. GAB1 is phosphorylated by ERK at four residues, which impairs the ability of constitutively active MEK to decrease p-AKT levels. The phosphorylated sites on GAB1 can recruit SHP2, leading to the dephosphorylation of RasGAP binding sites and regulation of the PI3K pathway (Lee et al).

PI3K-mTORC1 pathway can also be cross-activated by the Ras-ERK pathway. PI3K can be allosterically activated by the direct binding of Ras-GTP. When the RAS-ERK pathway is strongly activated, it can also activate mTORC1 by ERK and RSK signalling to the TSC complex.

mTORC1 signalling pathway also seems to be regulated by MAPK scaffolds. For the sustained activity of ERK, MEK1 scaffolding protein (MP1) is required, and MP1 also functions as a scaffolding protein for Ras GTPases. Therefore, MP1 may lead to cross-talk between two pathways by co-localising ERK and mTORC1 (Mendoza et al., 2011).

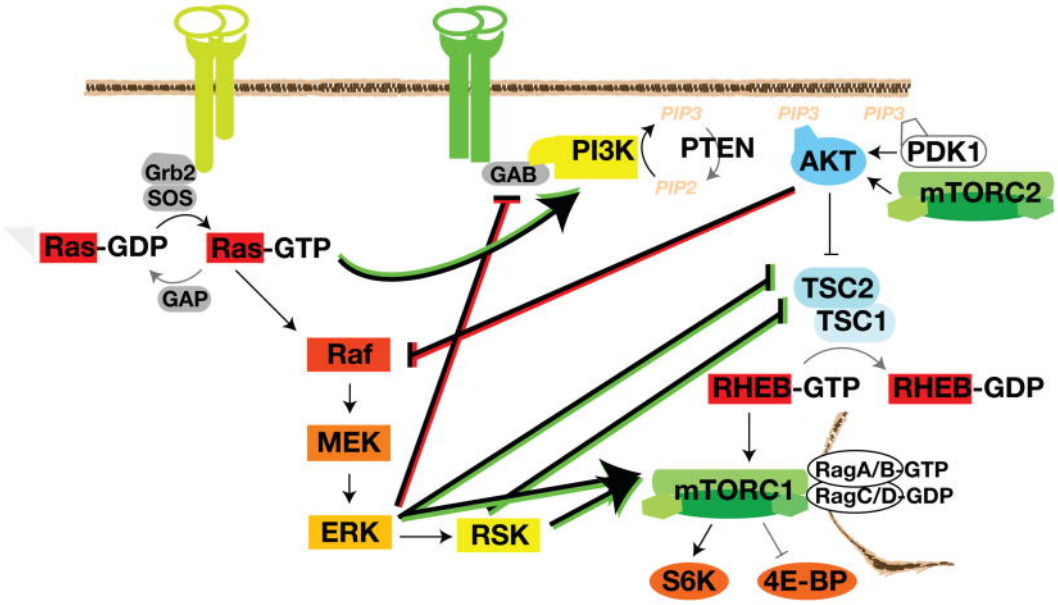

Figure 1.5.1.1 Crosstalk between PI3K and MAPK Pathways There are several signalling factors involved in both MAPK and PI3K pathway; it leads to a crosstalk between two signalling pathways. Figure is taken from Mendoza et al. 2011.

1.5.3 The Role of Crosstalk between MAPK and PI3K Pathways on Therapeutic Resistance

Since PI3K-mTORC1 and Ras/ERK pathways are majorly involved in the regulation of cell survival, proliferation, motility and metabolism activation of these pathways are commonly seen in oncogenesis. As a result of the crosstalk and pathway convergence, activated PI3K/mTORC1 and Ras/ERK signalling cascades may theoretically induce the resistance development

against the inhibitors targeting only one of the pathways (Di Nicolantonio et al., 2011).

1.6 Rationale and Aims of the Study

The FDA recently approved using the Fulvestrant-Alpelisib combination in PIK3CA mutant breast cancers. Clinical trials have shown that combinatory treatment approximately doubled the progression-free survival compared to single use of Fulvestrant in PIK3CA mutant breast cancers. However, due to the selective pressure exerted by the drug, certain tumour cell populations within the collective will dominate and be naturally selected, leading to the development of acquired resistance. Acquired resistance impairs the potency of the drugs and, as a result, decreases the survival rates of the patients. Unfortunately, resistance development against cancer therapies is still a major challenge. Moreover, the tumours that acquire resistance to the treatments generally grow more aggressively and able to metastasize.

This study focuses on the identification of factors which might contribute to the resistance development against Alpelisib-Fulvestrant combination in Luminal A breast cancer cell line models, MCF7 and T47D. We aim to offer an alternative therapeutic approach in case of acquired resistance.

2. MATERIALS AND METHODS

2.1 Materials

Table 2.1.1 Cell Culture Reagents and Media

Catalogue Number	Name	Company
31-053-028	Dulbecco's Modified Eagle Medium without phenol red	Gibco, USA
11-965-092	Dulbecco's Modified Eagle Medium High Glucose	Gibco, USA
04-121-1A	Fetal Bovine Serum	Biological Industries
TRY-1B10	Trypsin/EDTA	Thermo Scientific, USA
01-340-1B	MEM Non-essential Amino acids Solution	Biological Industries
P04-80100	L-Glutamine	Pan Biotech
PHA-H	Insulin	Capricorn
15-140-122	Penicillin-Streptomycin	Gibco
10131-035	G418 Solution	Gibco, USA
S2814	Alpelisib (BYL-719)	Selleckchem
1513857-77-6	Pemigatinib	Cayman Express
S1191	Fulvestrant	Selleckchem
68047-06-3	Tamoxifen	Cayman
116743.1000	Dimethyl Sulfoxide (DMSO)	Merck Millipore

Table 2.1.2 Cell Lines and Growth Media

Cell Line	Growth Media
MCF7 Parental	DMEM without phenol red, 1g/L D-Glucose, Pyruvate; 8% FBS, 1% Pen/Strep, 1% L-Glutamine, 1% NEAA 0.04% Insulin
MCF7 tamR	DMEM without phenol red, 1g/L D-Glucose, Pyruvate; 8% FBS, 1% Pen/Strep, 1% L-Glutamine, 1% NEAA 0.04% Insulin
MCF7 tamR fulvR BYLR	DMEM without phenol red, 1g/L D-Glucose, Pyruvate; 8% FBS, 1% Pen/Strep, 1% L-Glutamine, 1% NEAA 0.04% Insulin
T47D Parental	DMEM without phenol red, 1g/L D-Glucose, Pyruvate; 8% FBS, 1% Pen/Strep, 1% L-Glutamine, 1% NEAA 0.04% Insulin
T47D tamR	DMEM without phenol red, 1g/L D-Glucose, Pyruvate; 8% FBS, 1% Pen/Strep, 1% L-Glutamine, 1% NEAA 0.04% Insulin
T47D tamR fulvR BYLR	DMEM without phenol red, 1g/L D-Glucose, Pyruvate; 8% FBS, 1% Pen/Strep, 1% L-Glutamine, 1% NEAA 0.04% Insulin
HEK293	DMEM High Glucose (4.5 g/L), 8% FBS, 1% pen/strep

Table 2.1.3 Buffers and Solutions

Name	Ingredients
10X Transfer Buffer	30.3 gr Trizma base, 144.1 gr Glycine, completed to 1 liter with ddH_2O
10X Running Buffer	30 gr Trizma base, 144 gr Glycine, completed to 1 litre with ddH_2O
10X Tris-buffered Saline (TBS)	80 gr NaCl, 2 gr KCl, 30 gr Trizma-base completed to 1 L with ddH_2O, pH is adjusted to 7.4 with HCl
1X Tris-buffered Saline-Tween20	1 litre 1X TBS, 1 mL Tween20
Stacking Buffer (0.5 M Tris-HCl, pH: 6.8)	60.5 g Trizma-Base completed to 1 L with ddH_2O, pH is adjusted to 6.8 with HCl
Resolving Buffer (1.5 M Tris-HCl;, pH: 8.8)	187 g Trizma-Base completed to 1 L with ddH_2O, pH is adjusted to 8.8 with HCl
10% Resolving Gel	4.1 mL ddH_2O, 3.3 mL %30 acrylamide/bisacrylamide, 2.5 mL Resolving Buffer, 5 μL TEMED, 25 μL 10% APS
8% Resolving Gel	4.6 mL ddH_2O, 2.7 mL 30% acrylamide/bisacrylamide, 2.5 mL

	Resolving Buffer, 5 μL TEMED, 25 μL 10% APS
4% Stacking Gel	3 mL ddH_2O, 0.66 mL %30 acrylamide/bisacrylamide, 1.26 mL Stacking Buffer, 5 μL TEMED, 50 μL 10% APS
Blocking Buffer	5% BSA / 5% milk in TBS-T
50X TAE Buffer	242 gr Trizma-Base, 57.1 mL acetic acid, 100 mL 0.5 M EDTA
Urea Lysis Buffer	8 M urea in 20 mM HEPES (pH 8.0), 100 mM sodium orthovanadate, 500 mM sodium fluoride, 1M β-glycerol phosphate, 250 mM disodium pyrophosphate
Trichloro Acetic Acid Solution	50% TCA in ddH_2O,
Destaining Solution	10 mM Trizma-Base in ddH_2O
0.4% Sulforhodamine B	0.4% SRB in 1% acetic acid

Table 2.1.4 Kits, Reagents and Enzymes

Catalogue Number	Name	Company
G238	Mycoplasma Detection Kit	ABM, Canada
K-12045-D20	WesternBright ECL Kit	Advansta, USA
	BCA Protein Assay Kit	

P0758S	Sodium Orthovanadate	New England Biolabs, USA
62796-29-6	Sulforhodamine B	Thermo Scientific, USA
773301	PrimeStep Protein Ladder	BioLegend, USA
sc-2025	Anti-mouse IgG	Santa Cruz Biotechnology, USA
sc-2027	Anti-rabbit IgG	Santa Cruz Biotechnology, USA
G238	Mycoplasma Kit	Applies Biological Materials, Canada
740955.50	RNA Isolation Kit	Macherey-Nagel, Germany
169014875	Midi Kit	QiaGen, Germany
23391.02	Glycine	Serva, Germany

Table 2.1.5 Consumable Materials

Product Name	**Company**
10 cm Cell Culture Plate	SPL Life Sciences, Korea
6 cm Cell Culture Plate	SPL Life Sciences, Korea
6-well Cell Culture Plate	SPL Life Sciences, Korea
12-well Cell Culture Plate	SPL Life Sciences, Korea
96-well Cell Culture Plate	SPL Life Sciences, Korea
50 mL Falcon Tube	Isolab, Germany

15 mL Falcon Tube	Isolab, Germany
PCR Reaction Tube	Axygen, Corning, USA
1.5 mL Reaction Tube	Greiner Bio-One, Germany
1000 ul Pipette Tip	Plastigen, Spain
200 ul Pipette Tip	Genaxy, India
10 ul Pipette Tip	Greiner Bio-One, Germany
50 mL Serological Pipette	Sarstedt, Germany
25 mL Serological Pipette	Sarstedt, Germany
10 mL Serological Pipette	Sarstedt, Germany
5 mL Serological Pipette	Sarstedt, Germany
1.5 mL Cryovial Tube	SPL Life Sciences, Korea
Cell Scrapers	Isolab, Germany
Nitrocellulose Membrane	Amersham Life Sciences, UK
Whatman Filter Paper	GE Healthcare Life Sciences, USA

2.2 Methods

2.2.1 Cell Culture Maintenance and Passage

MCF7 and T47D cell lines were cultured in DMEM without phenol red, supplemented with 8% foetal bovine serum, 1% penicillin/streptomycin, 1% MEM non-essential amino acids, and 0.04% insulin. When the cells reached approximately 80% confluency, they were passaged at a 1/5 split ratio. Before using growth media, it was heated to 37°C with a water bath. The cell media was changed every three days; when the old media was removed, the cells were washed with 1X PBS solution and supplied with fresh media. To

passage the cells, the media was removed, the monolayer of the cells was washed with 2 mL of 1X PBS, and the cells were treated with 1 mL of trypsin/EDTA solution in a 37°C incubator for five minutes to detach the cells from the dish. After the cells were detached, 2 mL of cell media was added to inhibit trypsin activity. The cells were collected into a 15 mL Falcon tube and centrifuged for 5 minutes at room temperature at 1500 RPM. The supernatant was removed, the cells were resuspended in 1 mL of fresh media, and 200 μL of the suspension was seeded into a new cell culture dish. Cells were always maintained in a 37°C incubator with 5% CO_2.

2.2.2 Cell Thawing

The cryovial tube containing frozen cells was put into a 37°C water bath. After the cryovial content was melted, the cell suspension was transferred into a 15 mL Falcon tube. To dilute DMSO in the suspension, 2 mL of cell media was slowly added into the tube. The tube was centrifuged for five minutes at room temperature, 1500 RPM. DMSO containing supernatant was aspirated. The cell pellet was resuspended in 1 mL DMEM without phenol red, supplemented with 8% fetal bovine serum. The suspension was seeded into a 6 cm cell culture dish containing 3 mL of growth media.

2.2.3 Cell Freezing

The old media was aspirated from a 10 cm culture dish, and the monolayer of the cells was washed with 1X PBS solution. Cells were treated

with trypsin/EDTA solution for 5 minutes in a 37°C incubator. After the cells were detached, 2 mL of growth media was added, and cells were collected into a 15 mL Falcon tube. The tube was centrifuged for 5 minutes at room temperature, 1500 RPM. The supernatant was aspirated, and cells were resuspended in 3 mL freezing media composed of 40% DMEM without phenol red, supplemented with 50% foetal bovine serum and 10% DMSO as a cryoprotectant. The cells were transferred into three cryovials as 1 mL resuspensions. The cryovials were inserted into Mr. Frosty, a freezing container, and then placed into the -80°C freezer. The cryovials were transferred to a liquid nitrogen tank the following day.

2.2.4 Cell Counting with Haemocytometer

The procedure starts as if the cells were passaged till the step where the cells are collected into a 15 mL falcon tube. At that point, cells were tried to be separated from each other by pipetting up and down at least thirty times with a 1000 μM pipette. 15 μM of cell suspension was taken from the 15 mL falcon tube, transferred to a 1.5 mL tube, and thoroughly mixed with 15 μM trypan blue. 10 μM of trypan blue cell suspension mix was loaded to a haemocytometer. Cells located in each 16 square containing grids around the centre grid were counted. The cell number in each 16 square grid should not be below 60 and should not exceed 200, and the difference in the number of cells in different grids should not be more than 20. The average of four grids was taken. The average was multiplied by 2, which is the dilution ratio, and then multiplied by 10000, as indicated by the formula.

2.2.5 Inhibitor Treatment of the Cells

Cells were counted; for a 96-well plate, 3000 cells were seeded to each well. After one day, respective concentrations of Alpelisib, Pemigatinib or the combination of the two were provided to the cels. Cells were cultured for 5 to 7 days. When the DMSO control group reached approximately 100% confluency, treatment was ended. SRB cell viability assay was performed to assess the inhibitor effect.

2.2.6 Generation of Acquired Resistance in Cells

Tamoxifen resistant (Ward et al. 1173) MCF7 and T47D cell lines were kkind gifts from Professor Özgür Şahin. MCF7 tamR and T47D tamR cell lines were separated into two cohorts as doubling time control (DTC) and experimental (EXP). We treated the cells 1 μM, 2 μM, 5 μM, 20 μM and 50 μM doses of Fulvestrant to perform a dose escalation experiment. 1 μM, 5 μM, 10 um, 20 μM and 100 μM doses of alpelisib were used for MCF7 tamR cell line and 250 nM, 500 nM, 2.5 μM, 10 μM and 50 μM doses were used for T47D tamR cell line. IC_{20}, IC_{50}, IC_{70}, values for Alpelisib and Fulvestrant were calculated crystal violet cell viability assay was performed and IC_{20}, IC_{50}, IC_{70}, values for Alpelisib and Fulvestrant were calculated by using optical density (OD) values. The process was broken down into 5 periods and each period consisted of 6 weeks; making 30 weeks in total. DTC cells were treated only with fulvestrant while EXP cells were treated with both fulvestrant and tamoxifen. After each period ended, we made step-by-step increases in IC

values, as shown in Table 2.2.6.1. After the process is completed; we treated the cells with a maintenance dose of each drug to sustain the acquired resistance to the drugs. The IC_{50} doses that are determined before the acquired resistance process were used as maintanence dose.

Table 2.2.6.1: Schedule for Resistance Gaining Experiment Each period consists of six weeks. At the end of each period, the IC value of one of the drugs is increased to the upper one.

	Doubling Time Control Cells	**Experimental Cells**
Period 1	Fulvestrant IC_{20}	Fulvestrant IC_{20}
		Alpelisib IC_{20}
Period 2	Fulvestrant IC_{50}	Fulvestrant IC_{50}
		Alpelisib IC_{20}
Period 3	Fulvestrant IC_{50}	Fulvestrant IC_{50}
		Alpelisib IC_{50}
Period 4	Fulvestrant IC_{70}	Fulvestrant IC_{70}
		Alpelisib IC_{50}
Period 5	Fulvestrant IC_{70}	Fulvestrant IC_{70}
		Alpelisib IC_{70}

2.2.7 RNA Isolation

MCF7 tamR fulvR, MCF7 tamR fulvR BYLR, T47D tamR fulvR and T47D tamR fulvR BYLR cells were cultured. After cells reached approximately 80% confluency, cells were counted. 2.000.000 cells from

each cell line are transferred to a reaction tube and centrifuged for 5 minutes at room temperature, at 13.000 RPM. RNA isolation was performed with the Macherey Nagel NucleoSpin RNA Isolation kit, according to the manufacturer's instruction manual. RNA concentrations and quality were measured by NanoDrop.

2.2.8 RNA-Sequencing of the Cell Lines

Isolated RNA samples were sent to Gen Era Diagnostic Company for RNA sequencing. The quantity, quality and structural integrity of the total RNA were determined by capillary electrophoresis and fluorometric methods for quality control procedures. Measurements were performed by using the Qubit 3 fluorometer. Illumina Stranded Total Prep kit was used to prepare the library of isolated RNA material. The library preparation process was performed by following the manufacturer's instructions in the instruction manual. RNA sequencing was performed by using the Illumina NovaSeq 6000 next-generation sequencing platform. An average of 30 million 150 bp paired-end reads per sample was obtained in this step. Library quantification, dilution, and loading processes were conducted by following the manufacturer's relevant guidelines.

2.2.9 Stable Transfection and Viral Particle Production

HEK293 cells were used to perform transfection. Cells were counted; 800.000 cells were seeded into each well of a 6-well plate in 8% FBS containing DMEM. After 24 hours, the Lipofectamine3000 kit was used to

perform transfection; the instructions were followed, which are provided in the manufacturer's manual. After 24 hours, the media of the cells were replenished. Post 48 and 72 hours following the transfection, media of the cells were collected and transferred into 15 mL Falcon tubes wrapped in aluminium foil. Media were filtered with a 0.45 μM filter into 15 mL falcons, and falcons were wrapped with aluminium foil.

2.2.9 Retroviral Transduction of Cell Lines

The cells that were wanted to be transduced were seeded 24 hours before transduction at 20% confluency, obtained by seeding 240.000 cells per well of 6-well plates. On the day of transduction, media was aspirated and filtered, and viral particle-containing media was given to the cells. 10 ug/mL of polybrene was supplied to the media to ensure transduction efficiency.

2.2.10 Sulphorhodamine B Cell Viability Assay

After the treatment duration was ended, a 96-well plate which contained the cells was taken out from the incubator, and the growth media was poured into the sink by inverting the plate upside-down. 50 mL of 10% TCA solution was added into each well and incubated at room temperature for one hour to fixate the cells. Then, the fixation solution was poured into the sink; wells were washed with dH2O five times. The plate was air dried, 50 μM of SRB solution was added to each well, and the plate was covered with aluminium foil and incubated for 30 minutes at room temperature. SRB

solution was poured into the sink, and wells were washed with 1% acetic acid five times. The plate was air dried, and 200 μM of 10 mM Tris-base solution was added to each well to destain.

2.2.11 Urea Lysis

Lysis buffer and ice-cold PBS were prepared using the recipes provided in the materials section. When the cultured cells reached 80% confluency, they were washed with the ice-cold PBS for three times 500 μM of ice-cold lysis buffer was added into the plate, and cells were scraped with cell scrapers. Lysate was taken to 1.5 mL reaction tubes and kept on ice. Samples were sonicated at 40% amplitude for 15 seconds and rested for 25 seconds; the cycle was repeated three times. Sonication was also performed on ice. After sonication, lysates were centrifuged for 20 minutes at +4°C, 12.000 RPM. The supernatant was transferred to a fresh tube, and samples were snap-frozen in liquid nitrogen. Samples were stored at -80°C if they will be used later.

2.2.12 Protein Quantification

Protein quantification was performed with Pierce BCA Protein Assay kit according to the manufacturer's manual. BCA working solution was prepared by mixing each 50 units of Reagent A for 1 unit of Reagent B. 24 μL of sterile ddH2O was distributed to the wells; 1 μL of protein lysate was added, and 200 μL of the working solution was added to each well, by

pipetting up and down to mix thoroughly. The plate was incubated at 36ºC for 30 minutes, and optical density values were taken at 562 nM.

2.2.13 Spheroid Formation Assay

Cells were counted with a haemocytometer. 100.000 cells were seeded into 10 cm sterile bacteria plates, which are not cell culture treated. The plates supplied 8 mL of DMEM without phenol red were supplemented with 8% foetal bovine serum, 1% penicillin/streptomycin, 1% MEM non-essential amino acids, and 0.04% insulin. The cells were observed till they formed spheroid-like structures.

2.2.14 SDS-PAGE and Western Blot

Protein lysates were boiled for 5 minutes in a heat block adjusted to 95°C. Each lysate contained 20 ug/μM of protein, and 20 ul of protein was loaded into the wells of the gel. For protein electrophoresis, a Biorad Mini-Protean Hand-cast gel electrophoresis chamber was used. Running was performed in Tris-Glycine running buffer and was started at 90 volts till the proteins left the stacking gel. Voltage was increased to 100 while the samples were running in resolving gel. The run was continued until the samples reached the end of the gel.

After the run, proteins were transferred to a nitrocellulose membrane using a wet transfer method with a Tris-glycine-based buffer. The transfer was performed with 250 ampers for 2.5 hours, and the Biorad Mini-Protean system was used.

2.2.15 *In silico* Analyses

2.2.15.1 PANTHERdb

PANTHERdb is used to analyse high-throughput gene or protein data to classify and identify the function of gene products. We used PANTHERdb to visualise the enriched pathways for the differentially expressed genes in the resistant cell lines. The Reactome Pathway database was utilised to perform the analysis. *Homo sapiens* was selected for the organism, and results were generated as pie charts.

2.2.15.2 DAVID Analysis

DAVID is used to interpret the biological meaning behind a large set of genes by using different resources for functional annotation. It provides different parameters as output, including enrichment score and p-values. We used DAVID to identify the pathway enrichments in the resistant cell lines. Differentially expressed genes were pasted to the tool, “official gene symbol” was selected as the identifier, and Homo sapiens was selected as the organism. The Reactome Pathway, a functional annotation chart, was exported to form graphs.

2.2.15.3 STRING

STRING is used to identify the proteins which might be the interaction partners of each other. The differentially expressed genes are used to do the analysis, and *Homo sapiens* is selected for the “Organisms” parameter.

2.2.15.4 Arivis Cloud

To measure the spheroid areas, we used Arivis Cloud, an automated image analysis program. All the microscopy images are uploaded into the cloud, and a model is trained to identify spheroids in the images. Spheroids with regular sphere shapes are annotated as “spheroid class” to train the model. The ones with amorph in shape are annotated as the “amorph” class. Image backgrounds are also selected and annotated. The trained model outputted a results file that included all the counted “spheroid” and “amorph” classes with different specifications, including the areas of the classes. The “amorph” class is excluded from the analysis, and “spheroid” areas are analysed with GraphPad Prism to measure the average spheroid areas in case of different treatments.

2.2.16 Microscopy

To image spheroid cultures, a Leica DMi-8 microscope is used with LAS-X software to capture the images. 10x eyepiece and 4x lens were used to take the images, which makes a 40x magnification in total.

3. RESULTS

3.1 Determination of IC50 Values of T47D tamR and MCF7 tamR cells for Alpelisib and Fulvestrant

Endocrine therapy is used in hormone receptor-positive breast cancers. Patients who are allowed to use the Alpelisib-Fulvestrant combination as a treatment are likely to get hormone therapy before. Taking this into consideration, we wanted to use tamoxifen-resistant cell lines. We first wanted to check the tamoxifen responsiveness of the cells we use in order to validate that these cells are resistant to tamoxifen. We treated the cells with increasing doses of 4-hydroxy-tamoxifen (n=3), 100 nM, 200 nM and 300 nM. When DMSO control reached approximately 100% confluency, the experiment was ended, and a crystal violet cell viability assay was performed (Figure 3.1.1). We observed that tamR-resistant cell lines have an acquired resistance to tamoxifen compared to parental cell lines.

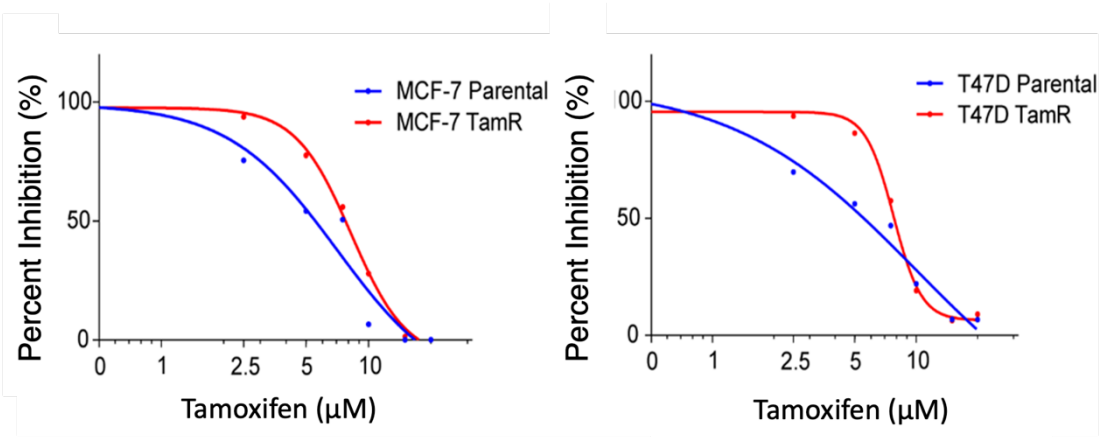

Figure 3.1.1 Percent Inhibition Graphs for Tamoxifen 1, 2.5, 5 and 10 μM doses of tamoxifen are used to perform dose escalation experiment. Cells are cultured in maintanence media, DMSO is used as vehicle. After the cells attached the treatment is started and continued until the DMSO controls reach to 80% confluency (approximately 7 days).

After confirming that the tamR cell lines have acquired tamoxifen resistance, we first needed to make the cells resistant to the Alpelisib-Fulvestrant combination. These cell lines were expected to be cross-resistant to Fulvestrant since tamoxifen and fulvestrant are both anti-oestrogens. They bind to ER and counteract the effects of oestrogen, thereby working as an agonist (Nathan et al., 2017). Tamoxifen is a selective oestrogen receptor modulator (SERM) (Movérare-Skrtic et al., 2014), while Fulvestrant is a selective oestrogen receptor degrader (SERD) (Fan et al. 20017). In order to develop resistance against Alpelisib-Fulvestrant cell lines, we determined IC_{20}, IC_{50}, IC_{70} and IC_{90} values of T47D tamR and MCF7 tamR cell lines for Fulvestrant and Alpelisib by crystal violet cell viability assay.

MCF7 Parental, T47D Parental and MCF7 tamR, T47D tamR cell lines were treated with 1 μM, 2 μM, 5 μM, 20 μM and 50 μM doses of Fulvestrant, control groups were treated with DMSO. Crystal violet cell viability assay was performed, and IC50 graphs for Fulvestrant were generated by GraphPad Prism with OD values at 586 nm (Figure 3.1.2).

For MCF7 cell lines, 1 μM, 5 μM, 10 um, 20 μM and 100 μM doses of Alpelisib was used. For T47D, 250 nM, 500 nM, 2.5 μM, 10 μM and 50 μM of Alpelisib were used. We determined IC20, IC50, IC70 and IC90 values of T47D tamR and MCF7 tamR cell lines for Fulvestrant and Alpelisib by crystal violet cell viability assay. IC50 graphs for Alpelisib were generated by GraphPad Prism (Figure 3.1.2). We observed that tamR cell lines have a cross-resistance against Fulvestrant.

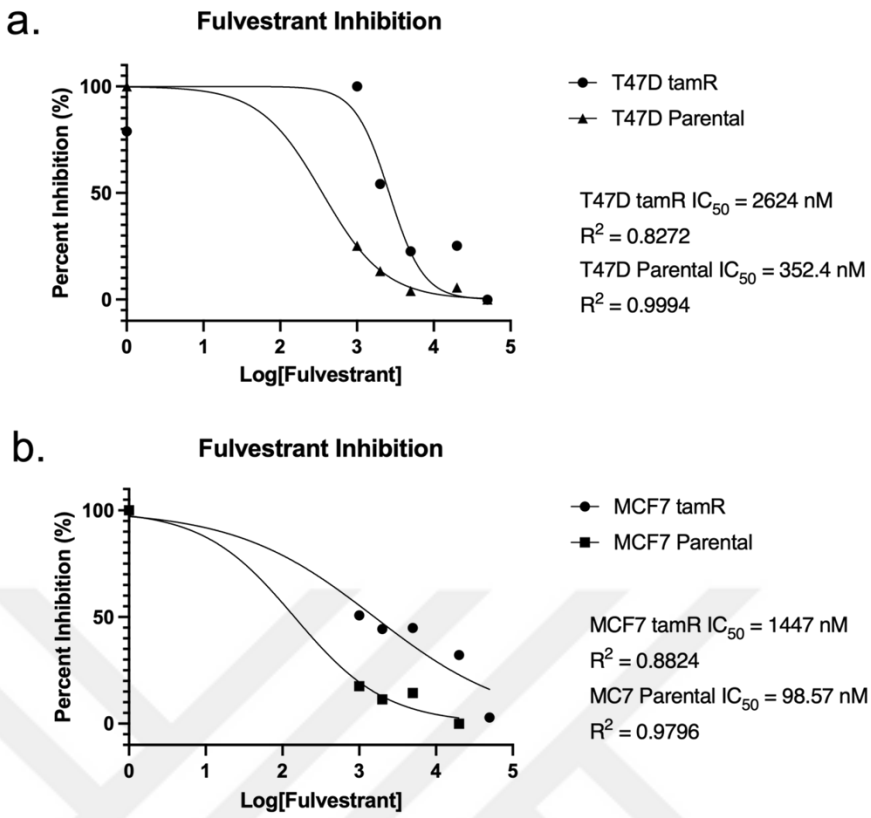

Figure 3.1.2: Fulvestrant Percent Inhibition Graphs a. T47D tamR versus T47D Parental b. MCF7 tamR versus MCF7 Parental. 1 μM, 2 μM, 5 μM, 20 μM and 50 μM doses of Fulvestrant was used to perform a dose escalation experiment, and cells were cultured in maintenance media. DMSO is used as the vehicle. After the cells attached the treatment is started and continued until the DMSO controls reach to 80% confluency (approximately 7 days).

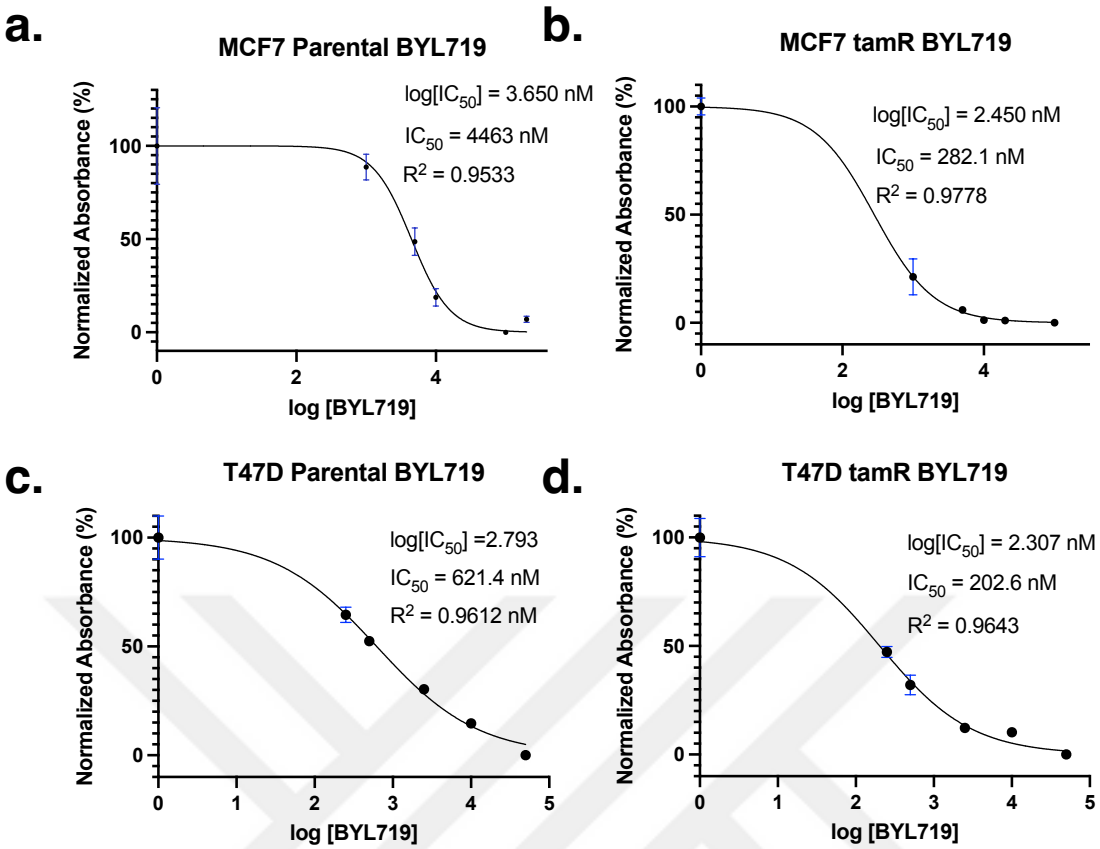

Figure 3.1.3: Alpelisib Percent Inhibition Graphs a. MCF7 Parental, b. MCF7 tamR; 1 μM, 5 μM, 10 um, 20 μM and 100 μM doses of Alpelisib (BYL719) were used c. T47D Parental, d. T47D tamR; 250 nM, 500 nM, 2.5 μM, 10 μM and 50 μM doses were used. DMSO is used as the vehicle, after the cells attached the treatment is started and continued until the DMSO controls reach to 80% confluency (approximately 7 days). Graphs are generated with GraphPad Prism, SEM was used to draw error bars.

3.2 Generation of Alpelisib-Fulvestrant Resistant MCF7 and T47D Cell Lines

To develop acquired Fulvestrant and ALPELISIB resistance, we divided T47D tamR and MCF7 cell lines into two cohorts: doubling time control and experimental cell lines. We treated doubling time control cell lines with increasing doses of only Fulvestrant. We treated experimental cell lines with increasing doses of both Fulvestrant and Alpelisib for a 30-week period,

as shown in Figure 3.2.1. We determined the dose-increasing schedule (Table 3.2.1) according to the IC20, IC50 and IC70 values of the corresponding drugs, as shown in Table 3.2.2

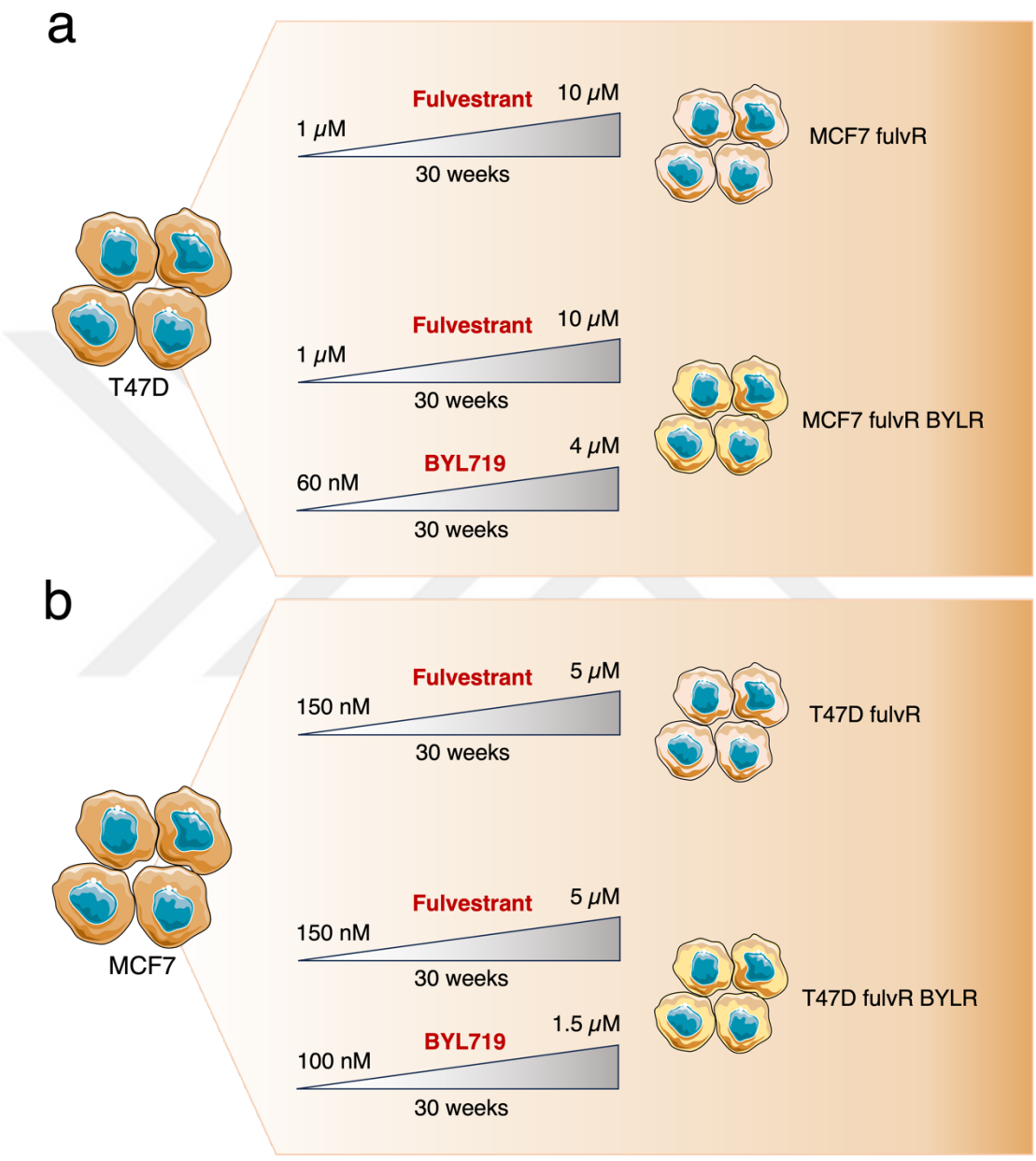

Figure 3.2.1 Generation of Acquired Resistance Both cell lines were resistant to tamoxifen; the cells were divided into two cohorts; doubling time control and experimental. Doubling time control cells were named as fulvR after the process was completed and the resistance was validated, while

experimental cells were named as fulvR BYLR after the validation. a. Process for MCF7 cell line. b Process for T47D cell line. (BYL719 is Alpelisib)

Table 3.2.2 IC_{20}, IC_{50}, IC_{70}, IC_{90} Doses of Each Cell Line

(nM)	Fulvestrant MCF7	Alpelisib MCF7	Fulvestrant T47D	Alpelisib T47D
IC_{20}	120.75	142.7	826	116.4
IC_{50}	1105	684.7	5624	896
IC_{70}	5476	1225	11476	4101
IC_{90}	10843	6079	42436	12980

In the first period, IC_{20} concentrations of both drugs are given to the cells. In the second period, the Fulvestrant dose was increased to IC_{50}, while the Alpelisib dose was kept at IC_{20}. In the second period, the Fulvestrant dose was kept at IC50; the Alpelisib dose was increased to IC_{50}. It is followed by step-by-step increases in IC_{50} and IC_{70} doses in six-week intervals, increasing only one drug concentration in each period.

3.3 Determination of IC50 Values After Resistance Gaining Process

After resistance gaining procedure has ended, MCF7 tamR and T47D tamR experiment cells and MCF7 tamR and T47D tamR control cells were treated with 0, 0.1, 0.2, 0.5, 1, 2, 5, 10, 20 and 50 μM doses of Alpelisib and 0.1, 0.5, 1, 2, 5, 20 and 50 μM doses of Fulvestrant. At the end of the

experiment, IC_{50} graphs for Alpelisib and Fulvestrant were generated for control and experiment cells with GraphPad Prism (Figure 3).

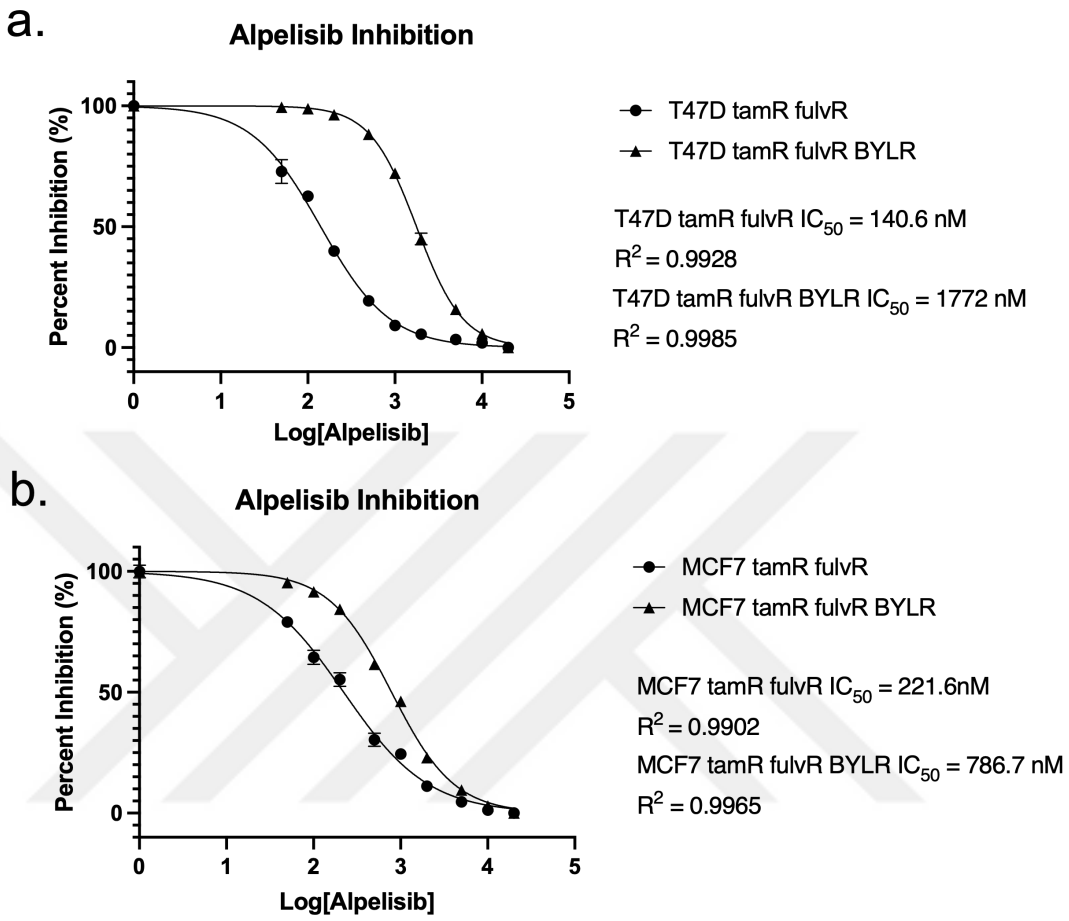

Figure 3.3.1 Alpelisib Percent Inhibition Graphs a. T47D tamR versus T47D Parental b. MCF7 tamR versus MCF7 Parental. 0.1, 0.2, 0.5, 1, 2, 5, 10, 20 and μM doses of Alpelisib was used to perform a dose escalation experiment, DMSO is used as the vehicle and cells were cultured in maintenance media until the DMSO control reaches 80% confluency.

As shown in Figure 3, IC_{50} values of MCF7 and T47D experiment cell lines increased approximately 2.5-fold compared to the control cell lines. From that point, the cells that acquired resistance against Alpelisib and Fulvestrant were named BYLR fulvR; the cells that acquired resistance against only Fulvestrant were named fulvR.

3.4 RNA Isolation and Sequencing of Alpelisib and Fulvestrant Resistant & Fulvestrant Resistant MCF7 tamR and T47D tamR Cells

To identify the changes in mRNA expression profile compared to the control (only resistant to Fulvestrant) after gaining resistance against the combination of Fulvestrant and Alpelisib, we extracted total RNA from the cells which are resistant to Fulvestrant and resistant to the combination of Alpelisib and Fulvestrant. Each cell line was cultured in 6 cm plates as three replicates till the cells reached approximately 80% confluency. Then, each cell line was counted with a haemocytometer; 3.000.000 cells from each T47D tamR fulvR replicate and T47D tamR fulvR BYLR replicates were transferred into the reaction tubes with proper labellings. 2.000.000 cells from each MCF7 tamR fulvR replicate and each MCF7 tamR fulvR BYLR replicate were also transferred into the reaction tubes with proper labellings. To isolate total RNA, the Macherey Nagel NucleoSpin RNA Isolation kit was used. After total RNA isolation, NanoDrop results of each sample were taken to assess the quality and quantity of the samples.

Table 3.4.1: NanoDrop Results of RNA Samples.

Sample Name	Nucleic Acid (ng/μM)	A260/A280	A260/A230	A260	A280
Blank	-0.244	-17.887	0.115	-0.006	0
T47D BYLR FulvR Rep1	688.623	2.11	2.2	17.216	8.161
T47D BYLR FulvR Rep2	705.816	2.103	2.072	17.645	8.392
T47D BYLR FulvR Rep3	761.763	2.069	2.188	19.044	9.204
T47D FulvR Rep1	487.901	2.034	2.141	12.198	5.997
T47D FulvR Rep2	403.542	2.037	2.132	10.089	4.954
T47D FulvR Rep3	519.833	2.104	2.256	12.996	6.178
MCF7 BYLR FulvR Rep1	361.206	2.087	2.146	9.03	4.327
MCF7 BYLR FulvR Rep2	554.482	2.166	2.191	13.862	6.4
MCF7 BYLR FulvR Rep3	442.049	2.083	2.151	11.051	5.304
MCF7 FulvR Rep1	491.838	2.04	2.17	12.296	6.028
MCF7 FulvR Rep2	537.823	2.07	2.158	13.446	6.496
MCF7 FulvR Rep3	284.61	2.052	2.172	7.115	3.468

The quality and quantity of the samples were in good condition according to the NanoDrop measurements. The samples were sent to RefGen Biotechnology Inc. with dry ice for RNA sequencing.

3.5 Quality Control of RNA Samples

The quantity, purity, and structural integrity of the samples were determined using fluorometric and capillary electrophoresis methods for quality control of the samples by RefGen Biotechnology Inc. (Figure 4). The

Qubit 3 fluorometer (Thermo Fisher, USA, #Q33216) and the 2100 Bioanalyzer (Agilent, USA, #G2939BA) were used in these measurements. In the gel electrophoresis image seen in Figure 2, migration of the samples without smearing indicates the integrity of the RNA. The bands aligned with the arrows correspond to 28S and 18S RNA.

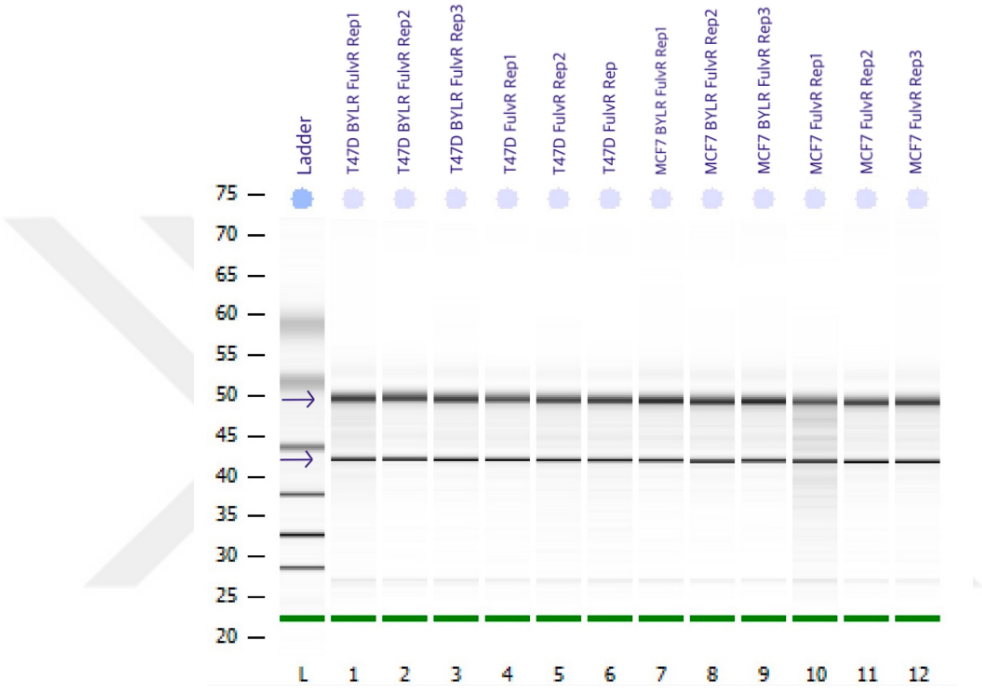

Figure 3.5.1: Gel electrophoresis image of the RNA sequenced samples. The arrows in the figure show 28S (upper one) and 18S (lower one) RNA.

RNA samples with RIN values between 7 and 8 exhibit good quality and integrity of genetic material (Schroeder, Andreas et al.). All RIN values for the samples presented in Figure 5 fall within this range, indicating their suitability for sequencing.

For library preparation, the company utilised the Illumina Stranded Total Prep kit (Illumina, USA, #20040534). This kit facilitated the removal of ribosomal

RNA from the samples, random fragmentation, and subsequent synthesis of primary and secondary cDNA strands. The library preparation process involved sequential steps of capture, fragmentation, RNA purification, cDNA synthesis, addition of index-barcode sequences, and purification.

Sequencing was performed using the Illumina NovaSeq 6000 next-generation sequencing platform. For each sample, a sequencing depth of 30 million reads with 150 bp paired-end reads was targeted. Quality control of the sequencing data was conducted using the FASTQC tool. Based on the quality control results, low-quality base reads and adapter contaminations were trimmed from the reads using the Trimmomatic tool (v0.39). The sequences obtained were aligned to the reference genome (Homo sapiens GRCh38.p13) using the HISAT tool (v2.1.0).

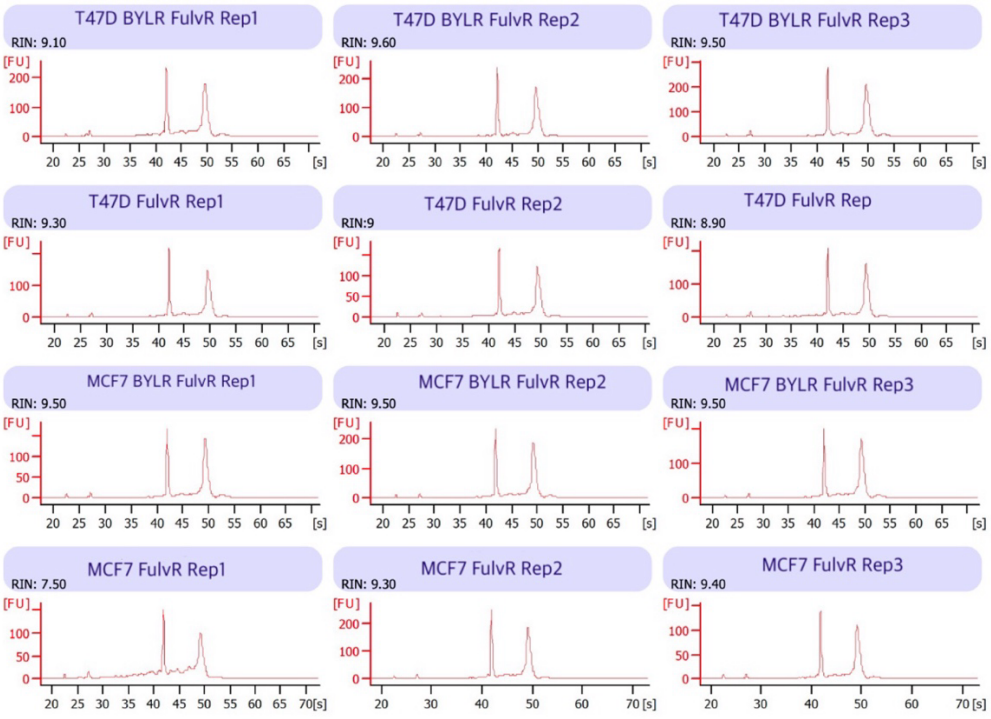

Figure 3.5.2: Electropherogram plots of RNA samples RIN scores of each sample are shown in the heading of the corresponding sample. Peaks correspond to the 28S (first peak) and 18S (second peak) RNA.

3.6 Comparative Transcriptome Analysis

3.6.1 Principal Component Analysis of RNA Samples

A Principal Component Analysis (PCA) plot was generated to evaluate the gene expression profiles of the samples. In this plot, it is observed that samples of the same cell type (biological replicates) cluster in similar locations, indicating that the profiles of these replicate samples are identical. The distinct positioning of each cluster suggests that the gene expression profiles of the cells that developed resistance against Alpelisib are different from those of the control cells. (Berglund, Anders E et al.).

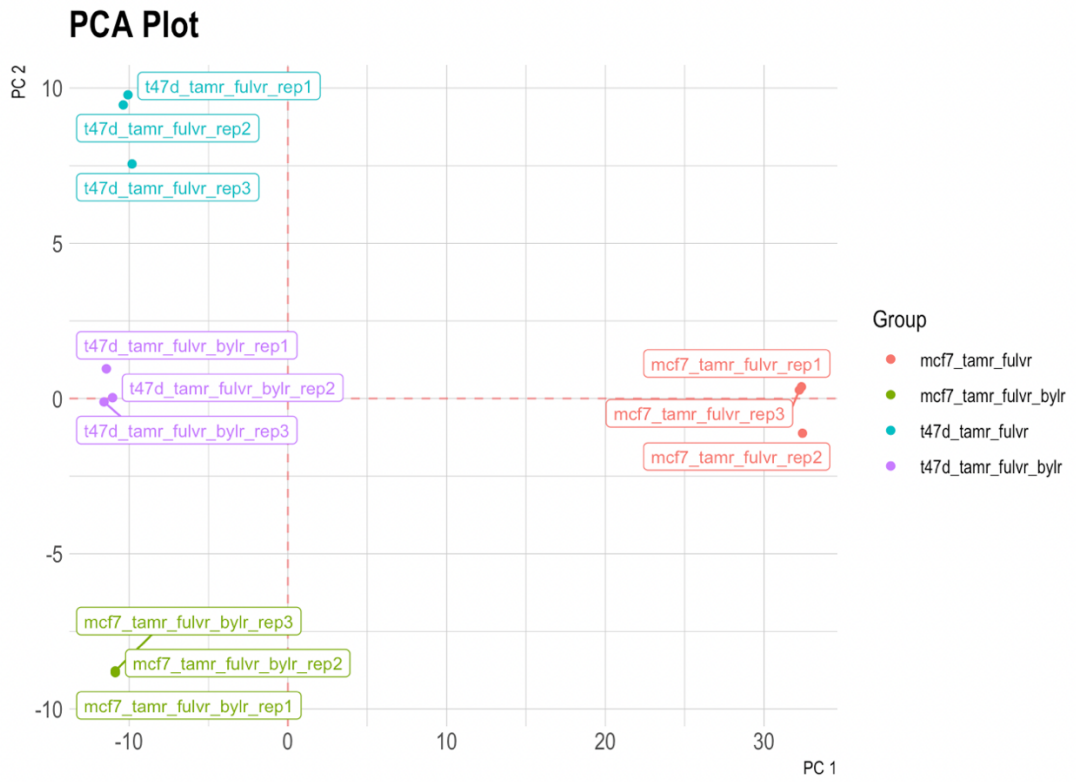

Figure 3.6.1.1: Principal component analysis of the RNA-sequenced samples Each dot represents a biological replicate, different colour represents different cell lines. The biological replicates of the same cell line clustered in similar locations.

3.6.2 Differential Expression Analysis

Differential expression analysis (DEG) determines the significant changes in expression profiles between experimental groups based on normalised read counts. In other words, it determines whether an observed difference in read counts for a particular gene is significant, meaning it is larger than expected by random variation. The number of genes which are significantly changed between experimental and control groups are shown in Table 3.6.2.1.

Table 3.6.2.1 Upregulated and Downregulated Gene Counts

Control Group	Experimental Group	Unchanged Genes	Upregulated Genes	Downregulated Genes
MCF7 tamR fulvR	MCF7 tamR fulvR BYLR	4121	2828	2750
T47D tamR fulvR	T47D tamR fulvR BYLR	6972	1360	1377

The list of differentially expressed genes for each comparison, which are listed according to the false discovery rate (FDR) values, was provided by RefGen Biotechnology Inc. We sorted both upregulated and downregulated genes for each cell line according to the logFC values. LogFC values were sorted from smallest to largest for the downregulated genes, while for the upregulated genes, they were sorted from largest to smallest. We filtered the genes with at least 4-fold changes ($|LogFC| \geq 2$) for both upregulated and downregulated genes. The second sorting criterion was the FDR value; only the genes with $FDR < 0.05$ are listed. Then, the lists were

compared to see the commonly differentially expressed genes in control and experimental groups of both cell lines.

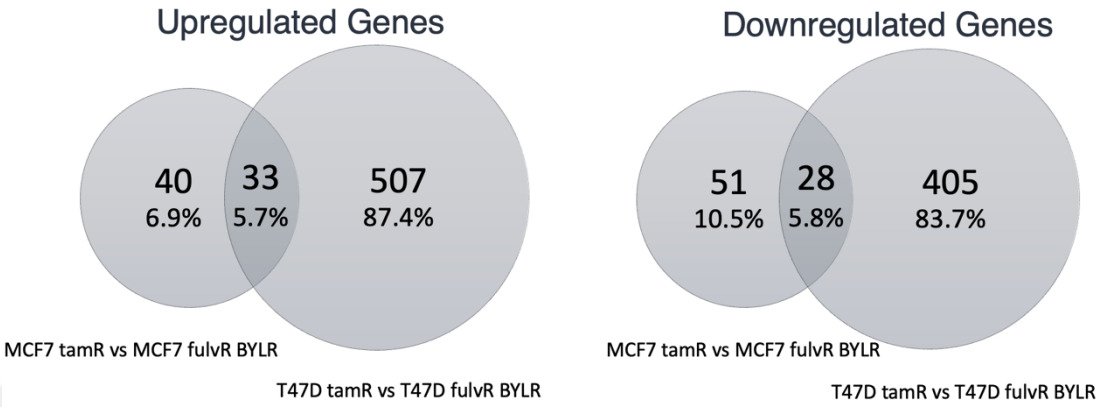

Figure 3.6.1.2 Venn Diagram The commonly differentially expressed genes are divided as upregulated and downregulated genes for T47D and MCF7 cell lines. False discovery rate (FDR) < 0.05; |LogFC| ≥ 2.

We observed that 33 (5.7%) of the genes are commonly upregulated, while 28 (5.8%) of the genes are commonly downregulated in MCF7 and T47D cell lines (Figure 3.5.1). We have done literature research on common differentially expressed genes to identify which genes might be responsible for developing resistance against Alpelisib. We listed the genes that might be the candidates for creating resistance.

3.6.3 Heatmap of PI3K Related Genes in Resistant Cells and Controls

We wanted to check the comparative expression levels of PI3K pathway-related genes to understand which molecules might be conferring resistance to alpelisib. PTEN which is the negative regulator of PI3K pathway, is downregulated and PIK3CA, PIK3CB, MTOR and RICTOR are

upregulated in T47D BYLR cell lines compared to the controls. PTEN, PIK3CA, PIK3CB, MTOR, RICTOR are upregulated and AKT1 is downregulated in MCF7 BYLR cell lines compared to the control cohorts.

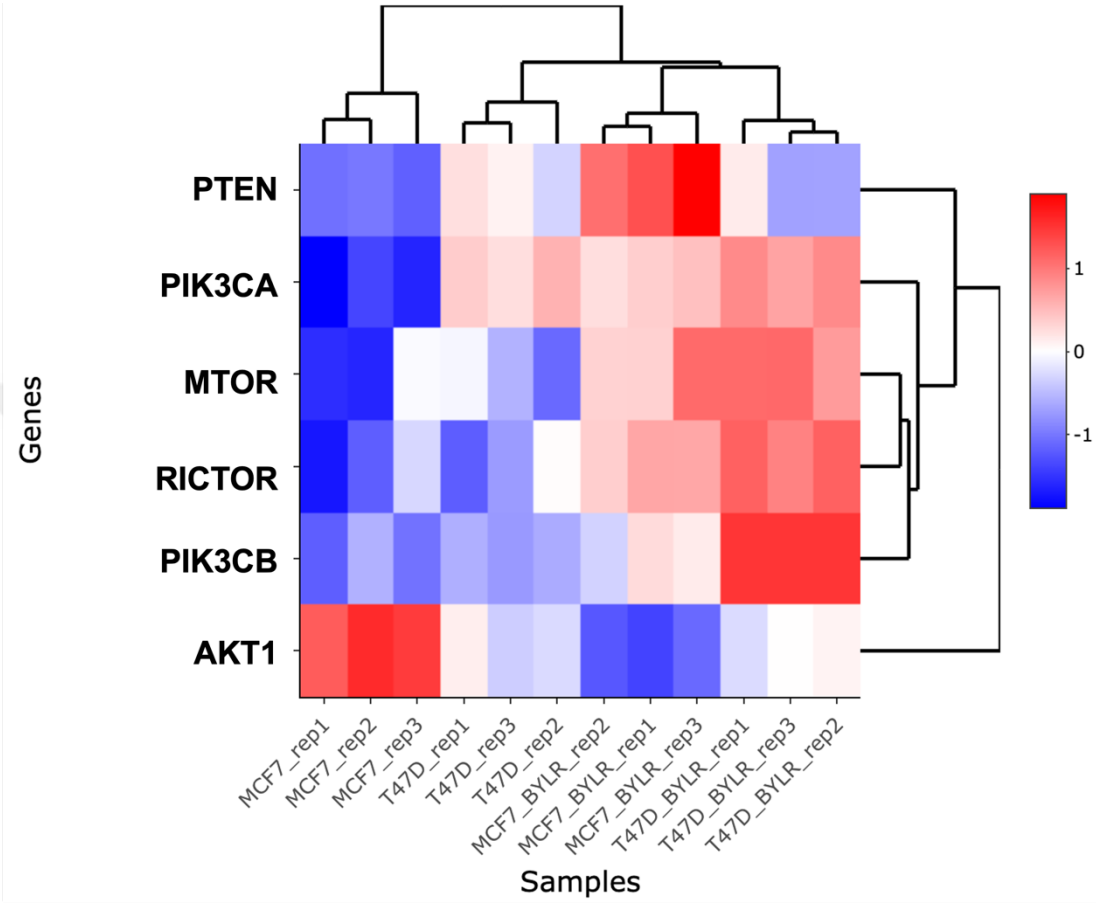

Figure 3.6.3.1 Heatmap of PI3K Pathway Genes PI3K pathway genes are shown in y axis; biological replicates of Alpelisib resistant cell lines and the controls are shown in x axis. Blue represents the downregulated genes; red represents the upregulated genes; numbers in the colour scale represent the fold change value. The differentially expressed genes with p value≤0.05 were used and expression data was $\log_2$ transformed.

We also checked the RAPTOR and PIK3CD genes to generate heatmap; however, after the filtering criteria these did not show significant changes among two cohorts.

3.7 *In silico* Analyses of the Differentially Expressed Genes

3.7.1 Pantherdb Pathway Analysis

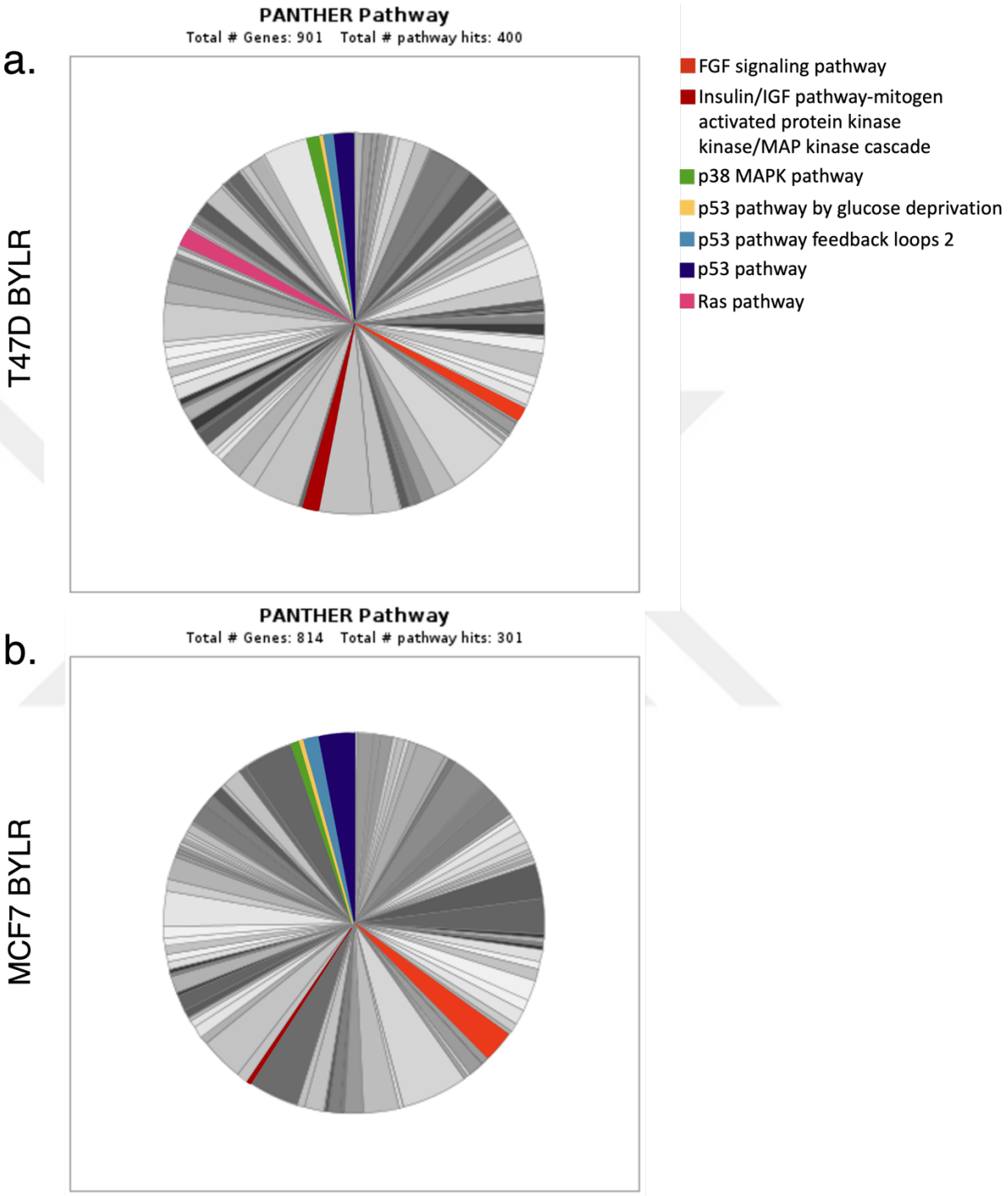

Figure 3.7.1.1 Pantherdb Gene Ontology Analysis of DEGs a. Pathway of DEGs in T47D BYLR cells b. Pathway analysis of DEGs in MCF7 BYLR cells. Legend is shown in the upper right panel.

We performed a Pantherdb Gene Ontology analysis with differentially expressed genes with 4-fold upregulation and downregulation (logFC≤-2 or logFC≥2) for T47D cell lines. In other words, we used the list of the genes that are upregulated 4-fold or downregulated 4-fold in T47D BYLR cell lines compared to T47D fulvR doubling time control cohort. Pathway ontology analysis is selected from the dropdown menu. The analysis included 901 genes and had 400 pathway hits. We observed that differentially expressed genes are involved in, FGF signalling pathway, Insulin/IGF pathway-mitogen activated protein kinase MAP kinase cascade, p38 MAPK pathway, p53 pathway by glucose deprivation, p53 pathway feedback loops 2, p53 pathway and Ras pathway (Figure 3.7.1.1a).

For MCF7 BYLR cell lines, we used the genes which are 2-fold upregulated or downregulated compared to the control cohort (logFC≤-1 or logFC≥1) because, in MCF7 BYLR cell lines, differential expression rates were not as high as T47D BYLR cell lines. Pathway analysis included 814 genes and 301 pathway hits. We observed that the same pathways are highlighted in MCF7 BYLR cell lines compared to their control, except for the Ras pathway.

3.7.2 DAVID Analysis

We performed a Database for Annotation, Visualization and Integrated Discovery (DAVID) analysis with differentially expressed genes in the alpelisib resistant cell lines compared to their control to visualise enriched pathways along with the enrichment and the corresponding p-values

(Sherman et al., Huang et al.). Results are visualised with bubble plots by the SRplot website (Tang et al.). Bubble size represents the number of the DEGs involved in the enriched term. P-values are -$\log_{10}$ transformed, so the greener the colour, the higher the significance and the x-axis shows the enrichment score. For T47D cell lines, DEGs with a 4-fold upregulation or downregulation rate were input to the DAVID tool; for MCF7, the genes with a 2-fold upregulation and downregulation rate were used. The signalling pathways, which include MAPK and FGFR pathway members, are used to plot the figures.

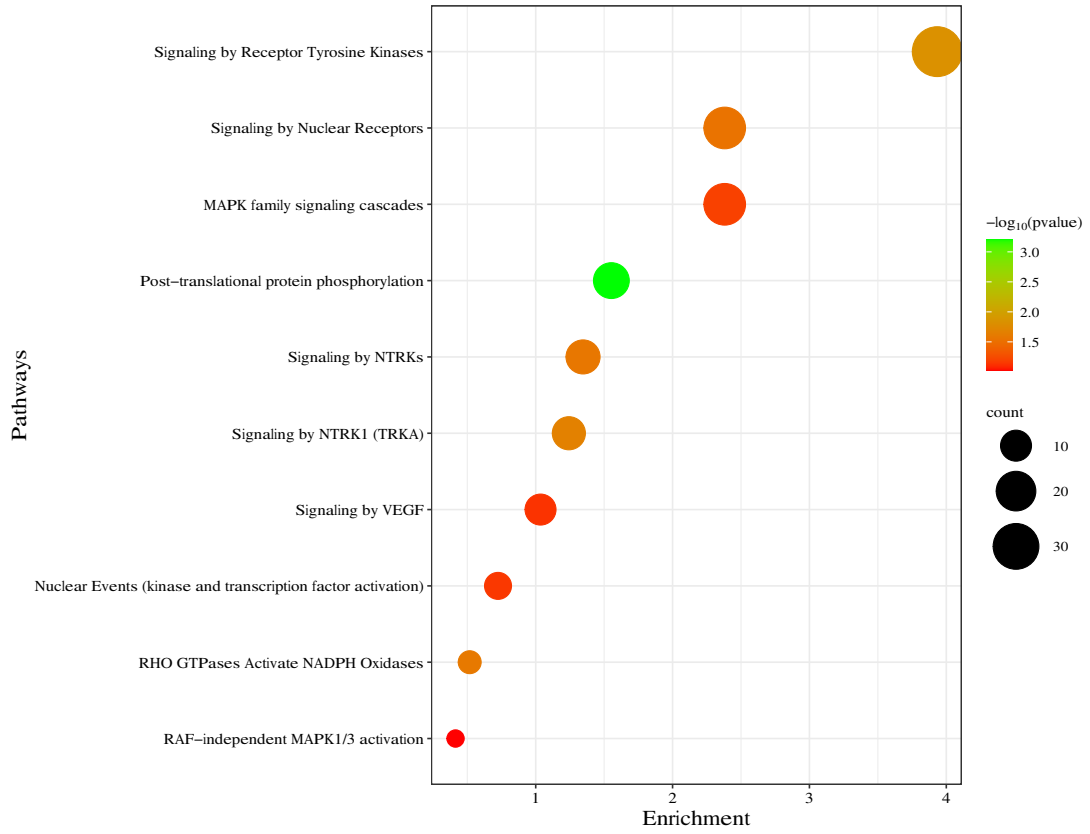

Figure 3.7.2.1 Bubble Plot of DAVID Reactome Pathway Enrichment Analysis of T47D BYLR Cell Line

In Figure 3.7.2.1, we observed that “Signalling by Receptor Tyrosine Kinases” had the highest enrichment score, suggesting that, while cells acquire resistance against Alpelisib, this pathway is one of the most affected since it involves many DEGs. We also see that “post-translational protein phosphorylation” events are enriched with a highly significant p-value. All the terms in Figure 3.7.2.1 involve the activity of MAPK pathway members.

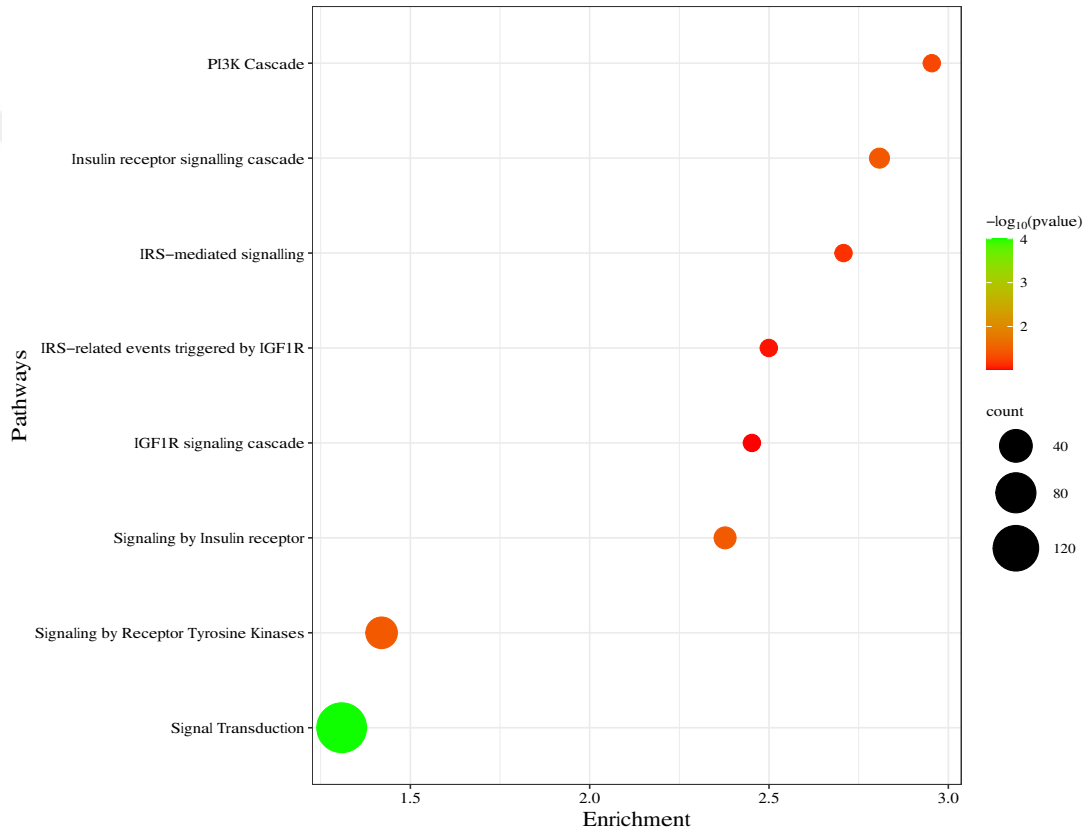

Figure 3.7.2.2 DAVID Reactome Pathway Enrichment Analysis of MCF7 BYLR Cell Line

Figure 3.7.2.1 shows the terms enriched for MCF7 BYLR cell lines. In this analysis, we observed an enrichment of the terms that involve the activity of FGFR pathway members. In Figure 3.7.2.1, it is observed that signal

transduction is the most significantly enriched term, and the DAVID analysis shows that it involves FGFR3 and FGFR4 activity along with FGFRL1.

3.7.3 Cytoscape ClueGO Analysis

After finding the enriched pathways in differentially expressed genes, we wanted to perform a detailed analysis to see a network-based visualisation of the differentially expressed genes. We used the same gene lists used in Pantherdb and DAVID analysis to perform ClueGO analysis (Bindea et al.). Reactome Pathway database (25.05.2022) is used to perform the analysis, and a detailed network specificity is chosen with GO tree interval levels of minimum=7 and maximum=15. The enriched terms are filtered to see the pathways, including MAPK activity (Figure 3.6.3.1). Parallel to the results we obtained from Pantherdb and DAVID analysis, we observed that differentially expressed genes are involved in the signalling events that regulate the MAPK pathway for T47D alpelisib-resistant cell lines (Figure 3.6.3.1).

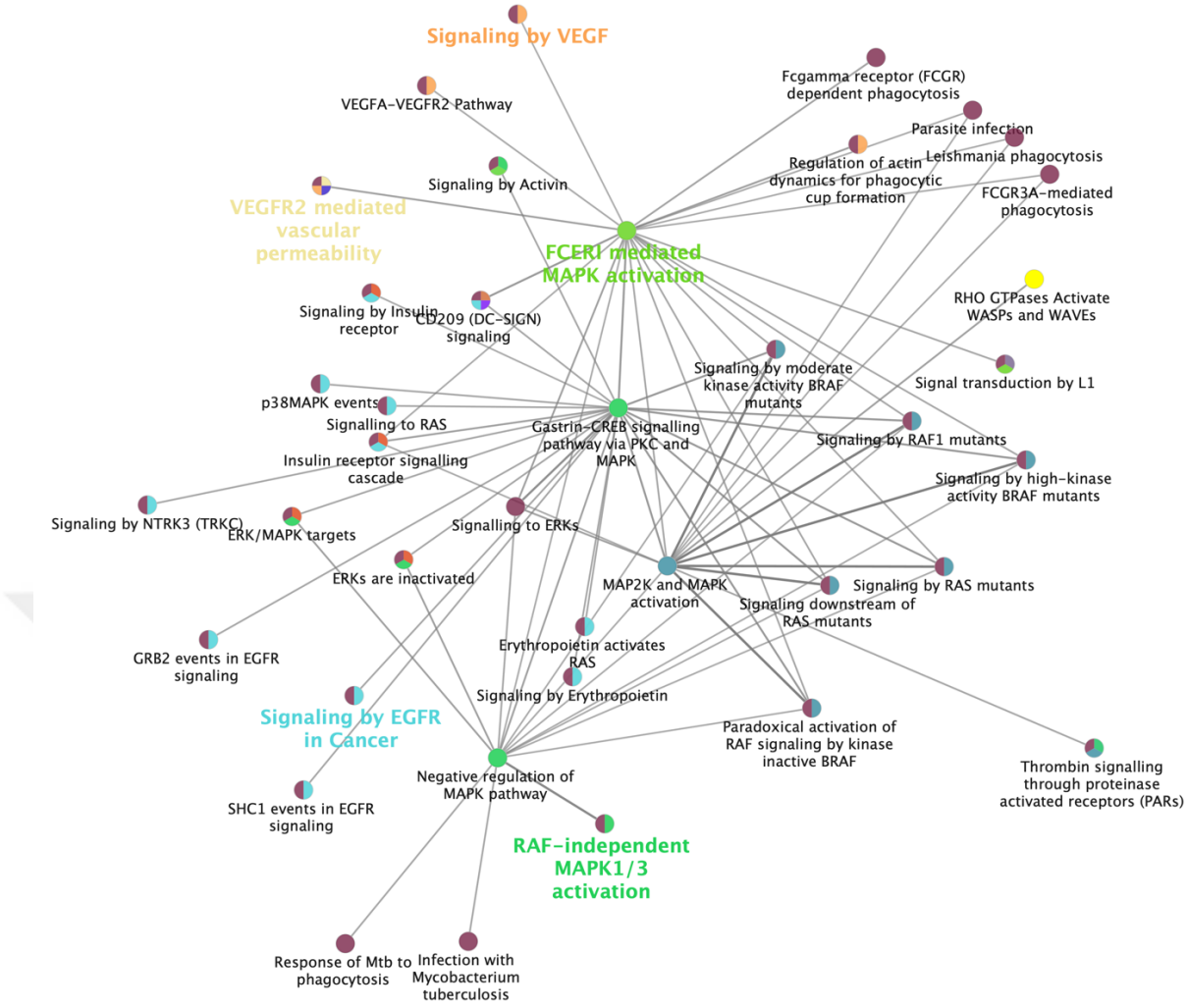

Figure 3.7.3.1 Cytoscape ClueGO Analysis of DEGs in T47D BYLR Cells
Differentially expressed genes with |logFC| ≥ 1 are used for mapping.

Reactome Pathway database (25.05.2022) is used to perform the analysis, and a detailed network specificity is chosen with GO tree interval levels of minimum=5 and maximum=10. The enriched terms are filtered to see the pathways, including MAPK and FGFR cascade activity (Figure 3.6.3.2). Parallel to the results that we obtained from Pantherdb and DAVID analysis, we observed that differentially expressed genes are also involved in

the signalling events which regulate the MAPK pathway for MCF7 and alpelisib-resistant cell lines (Figure 3.6.3.2 a).

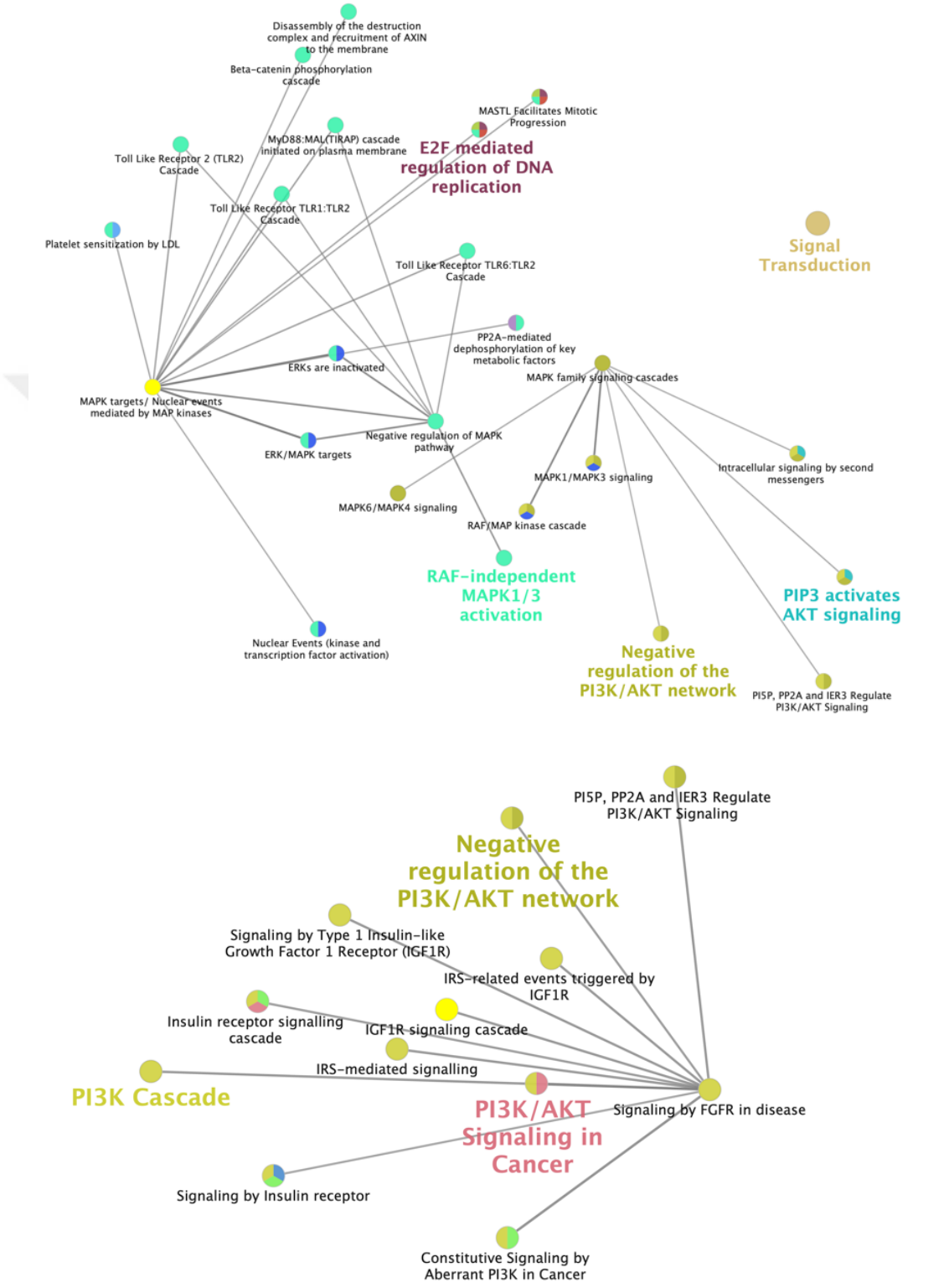

Figure 3.7.3.2 Cytoscape ClueGO Analysis of DEGs in MCF7 BYLR Cells

Differentially expressed genes with |logFC| ≥ 2 are used for mapping.

MCF7 cell lines also showed an enrichment for the FGFR pathway (Figure 3.6.3.2). It is observed that PI3K regulation seems to be taking place through FGFR signalling (Figure 3.6.3.2). IRS and IGF1R signalling are also activated by enrichment of the FGFR signalling pathway.

3.7.4 STRING Analysis

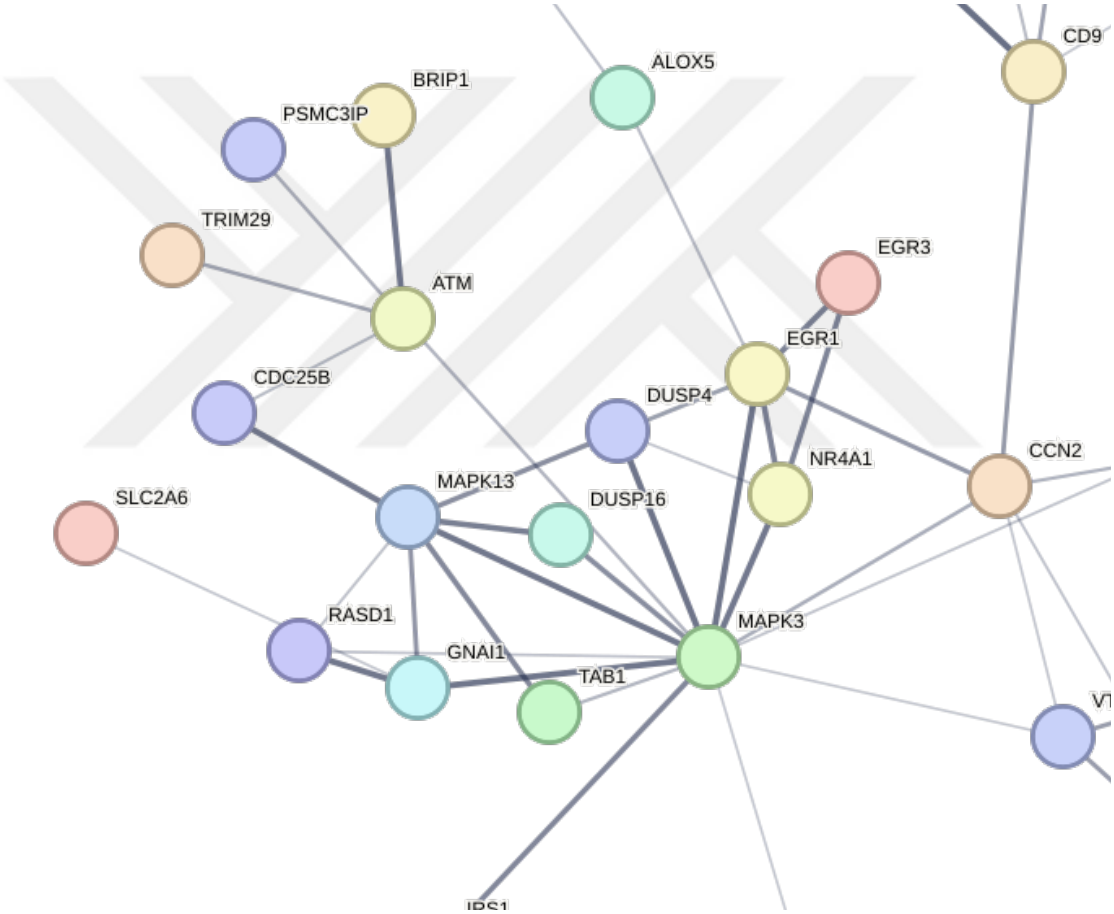

Figure 3.7.4.1 STRING Analysis of Common DEGs with MAPK Components The common DEGs are used to generate the map.

We wanted to perform a STRING analysis to see the interaction partners of the protein-coding genes, which are differentially expressed in the

cells that acquired resistance against alpelisib. We used common DEGs in MCF7 and T47D alpelisib resistant cell lines to perform the STRING analysis. Figure 3.7.1 shows that the proteins involved in the MAPK pathway are both differentially expressed in the resistant cells and interact with the other differentially expressed protein-coding genes. Therefore MAPK pathway proteins might have a common expression pattern for both MCF7 and T47D Alpelisib-resistant cell lines.

3.8 MAPK Downstream Proteins are Upregulated in Resistant Cell Lines

We identified many genes involved in the MAPK signalling pathway as a result of the literature research and *in silico* analyses. Therefore, we wanted to check the expression levels of the proteins that take place in MAPK signalling to validate the upregulation of these proteins at the translational level. MAPK, Phosphorylated MAPK (p-p44/42 Tyr202/204 and p-p44/42 Tyr204), p-PRAS, S6 and p-S6 (Ser235/236), KRAS and p53 protein expression levels are analysed by Western Blotting. We observed that levels of MAPK are significantly increased in the cells that developed resistance against Alpelisib. Moreover, phosphorylated forms of MAPK are also increased in both cell lines. Therefore, we confirmed that Alpelisib-resistant cell lines might exploit the MAPK pathway to overcome PI3K inhibition.

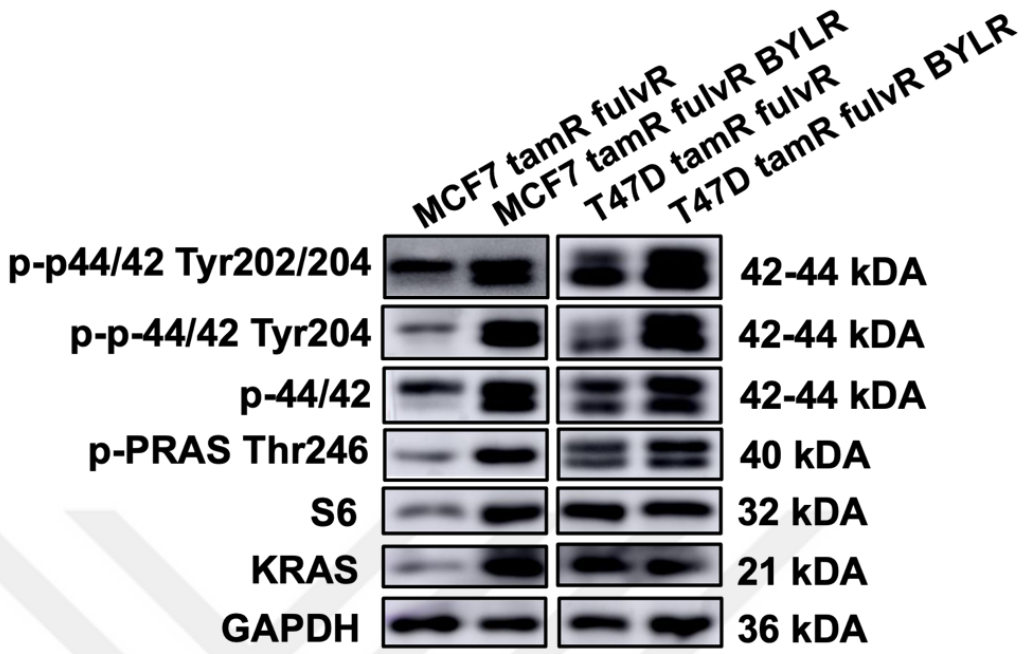

Figure 3.8.1 Western Blot of Non-Resistant and Resistant T47D and MCF7 Cell lines. 20 μg of protein was loaded into each well. Samples were run in 10% gel and GAPDH was used as a loading control.

According to the signal intensity measurements of the bands by Fiji. Phosphorylated MAPK (p-p44/42) Tyr202/204 level is increased 1.6 fold in resistant cell lines. Phosphorylated MAPK Tyr204 increased 11-fold in MCF7 BYLR cells, while it increased 4.6-fold in T47D BYLR cells. Total MAPK (p44/42) is upregulated by a 2.8-fold ratio in MCF7 BYLR compared to its control, while In T47D, it is increased 1.7-fold.

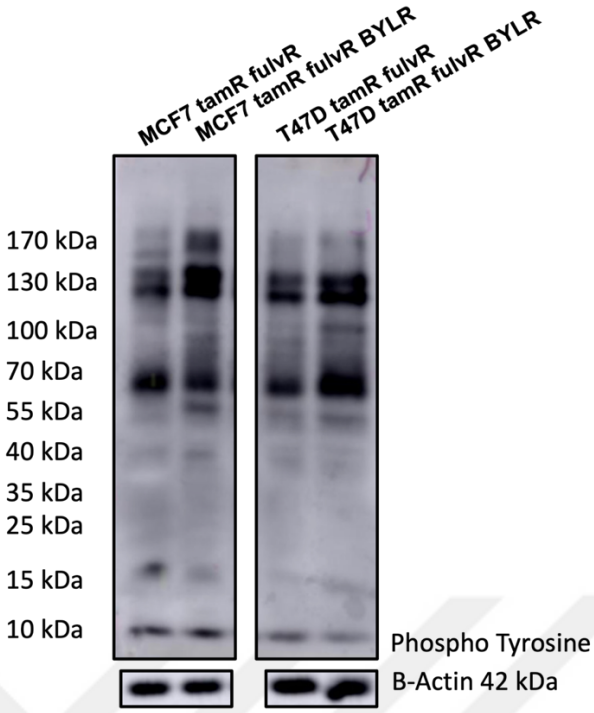

Figure 3.8.2 Western Blot of Phospho-Tyrosine Substrates 20 μg of protein, was loaded into each well. The samples were run in 10% gel. β-Actin panel was used as a loading control.

3.9 Synergistic Effect of Pemigatinib and Alpelisib Treatment in 2D Growth Inhibition

The MAPK pathway is activated in the cells, which developed resistance against Alpelisib. Since the MAPK pathway can be activated via FGFRs, we wanted to combine an FGFR inhibitor with a basal inhibition level of Alpelisib. We wanted to see if FGFR inhibitor and p110 alpha inhibitor alpelisib combinatory treatment synergistically inhibit the growth of MCF7 BYLR and T47D BYLR cell lines. We used 750 nM of Alpelisib for T47D BYLR and MCF7 BYLR cell lines to inhibit the overactivation of the PI3K pathway; in combination, we used increasing doses of Pemigatinib as 500

nM, 800 nM, 1 μM, 2 μM, 5 μM, and 10 μM. SRB cell viability assay was performed after the DMSO control group reached 100% confluency.

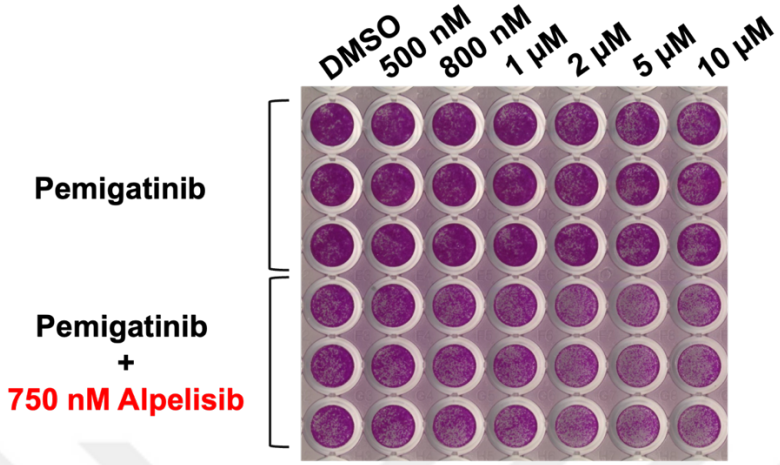

Figure 3.9.1 SRB Staining Image of T47D BYLR Cells. DMSO is used as the vehicle to deliver inhibitors. 3000 cells were seeded into each well. Cells were cultured in maintenance media with the indicated doses of inhibitors till the DMSO control group reached 80% confluency. Cells were treated with increasing doses of only Pemigatinib (upper triplicates) and 750 nM alpelisib and increasing doses of Pemigatinib. Each dose is treated in triplicates.

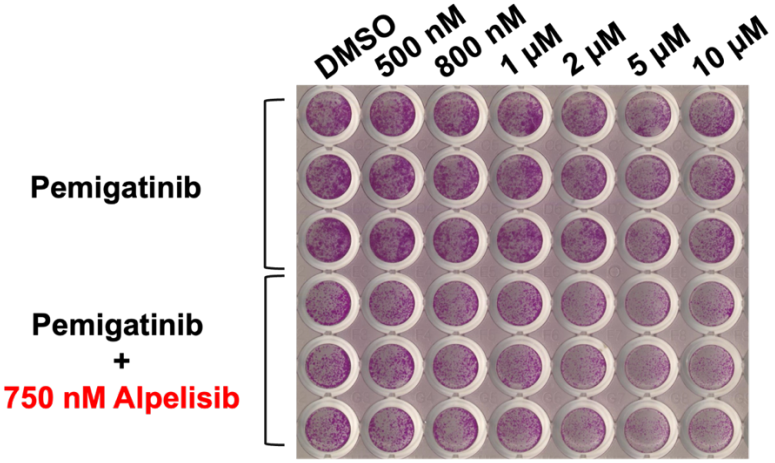

Figure 3.9.2 SRB Staining Image of MCF7 BYLR Cells. DMSO is used as the vehicle to deliver inhibitors. 3000 cells were seeded into each well. Cells were cultured in maintenance media with the indicated doses of inhibitors till the DMSO control group reached 80% confluency. Cells were treated with increasing doses of only Pemigatinib (upper triplicates) and 750 nM alpelisib and increasing doses of Pemigatinib. Each dose is treated in triplicates.

We also calculated the combinatory index for each combination with the formula provided below.

$$CI\ Value\ =\ \frac{\frac{Combination\ Treatment\ OD\ value}{Control\ OD\ Value}}{\frac{Alpelisib\ Only\ OD\ Value}{Control\ OD\ Valuue} \times \frac{Pemigatinib\ Only\ OD\ Value}{Control\ OD\ Value}}$$

Table 3.9.1 CI Values of Different Combinations of Pemigatinib with 750 nM alpelisib. Synergy index (CI) values are separately shown for MCF7 and T47D cell lines.

MCF7 BYLR					
Drug Combination	750 nM BYL719 + 500 nM Pemigatinib	750 nM BYL719 + 800 nM Pemigatinib	750 nM BYL719 + 1 µM Pemigatinib	750 nM BYL719 + 2 µM Pemigatinib	750 nM BYL719 + 5 µM Pemigatinib
CI Value	0.87	0.7	0.6	0.56	0.52

T47D BYLR					
Drug Combination	750 nM BYL719 + 500 nM Pemigatinib	750 nM BYL719 + 800 nM Pemigatinib	750 nM BYL719 + 1 µM Pemigatinib	750 nM BYL719 + 2 µM Pemigatinib	750 nM BYL719 + 5 µM Pemigatinib
CI Value	0.96	0.77	0.77	0.63	0.53

When the CI value of two drugs is smaller than 1 (CI<1), it means the combination of two drugs shows a synergistic effect on growth inhibition; if CI is equal to 1 (CI=1), the effect of the two drugs is additive and if CI value is larger than 1 (CI>1) the combination of two drugs shows the antagonistic effect (Chou, 2018). Considering these values, we showed that the combination of alpelisib and Pemigatinib shows a synergistic effect on MCF7 BYLR and T47D BYLR cell lines.

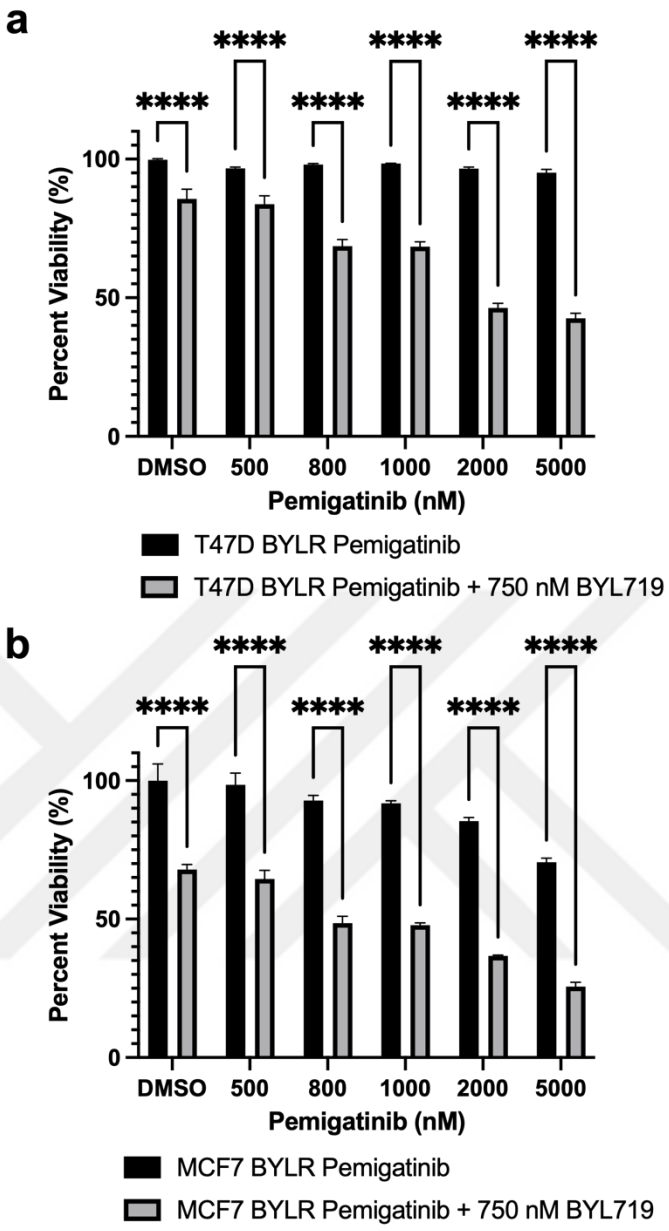

Figure 3.9.3 Percent Viablity Graphs for MCF7 BYLR and T47D BYLR
Percent inhibition is determined by absorbance values at 564 nm. Error bars were drawn by using SEM. 2-way ANOVA is used for comparisons. . P values for ****≤ 0.0001, ***≤ 0.001, **≤ 0.01, *≤ 0.05, ns ≤ 005

We observed that when only Pemigatinib is used to inhibit cell growth, it was not successful at all for the T47D BYLR cell line, while it only inhibited the growth of MCF7 BYLR cell lines by approximately 25%. However, when 1μM of alpelisib is combined with Pemigatinib, inhibited the growth of T47D

BYLR cell lines up to 60% for 1 μM alpelisib + 5 μM of Pemigatinib combination. On the other hand, the 750 nM alpelisib + 5 □M combination also significantly inhibited the growth of the MCF7 BYLR cell line, with a ratio of approximately 75%.

3.10 Pemigatinib and Alpelisib Combination is Effective to Inhibit 3D Growth of the Cell Lines

To investigate the inhibitory effect of the Pemigatinib + alpelisib combination in 3D growth of the T47D BYLR cells, we performed a spheroid formation assay and treated the cells with different doses of Pemigatinib and its combination with alpelisib; the experiment setup is shown in Figure 3.7.1.

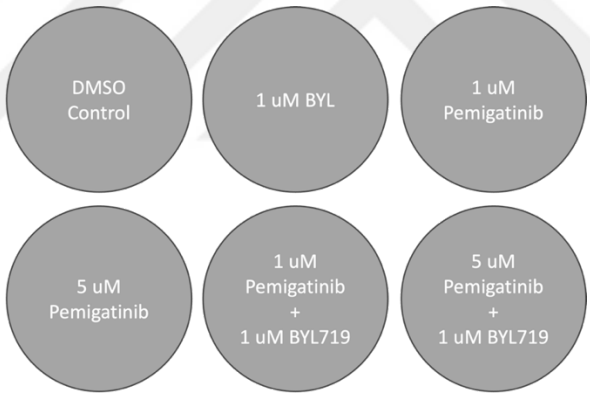

Figure 3.10.1 Experimental Setup for Spheroid Formation and Inhibition Experiment The treatment doses are indicated in each well.

Cells were seeded on day 0, and drugs were given on day 1. Cells were checked every day until the first spheroids started to form. Spheroids started to form on day 3, and from day 3, photographs of the culture were taken every 2 days. Ten photographs of each condition were taken every day. Representative images of each condition for both cell lines were given in Figure 3.8.2 and Figure 3.8.3

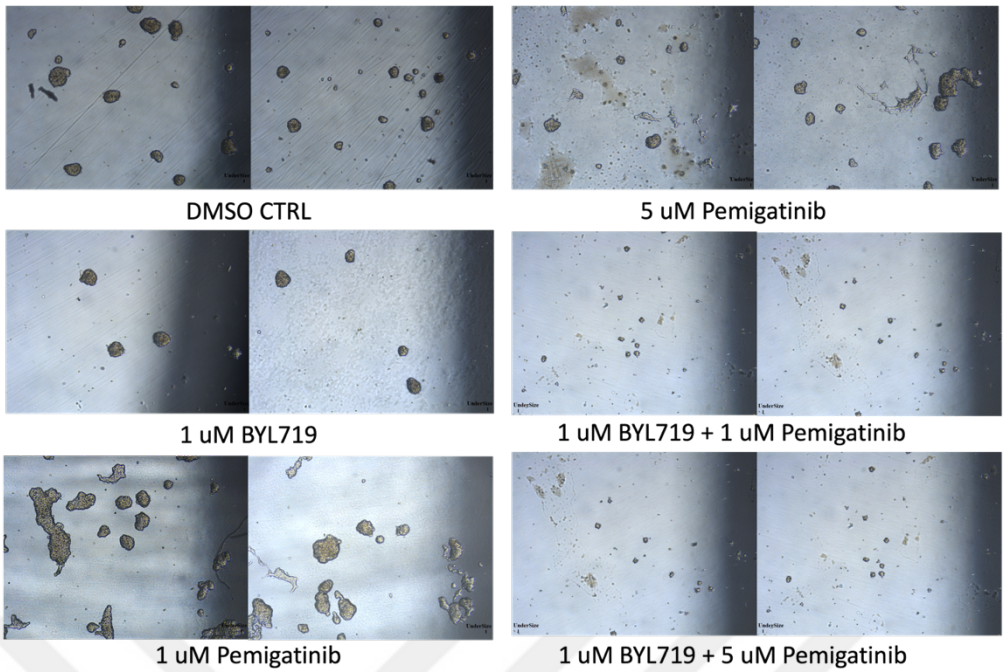

Figure 3.10.2 Microscopy Images of T47D BYLR Spheroids Images are acquired with LAS-X Software with Leica DMi8 Microscope. 5x Lens is used along with 10x eyepiece lens, (40x magnification). Cells were cultured in maintanence media with the indicated doses of the inhibitors for 10 days.

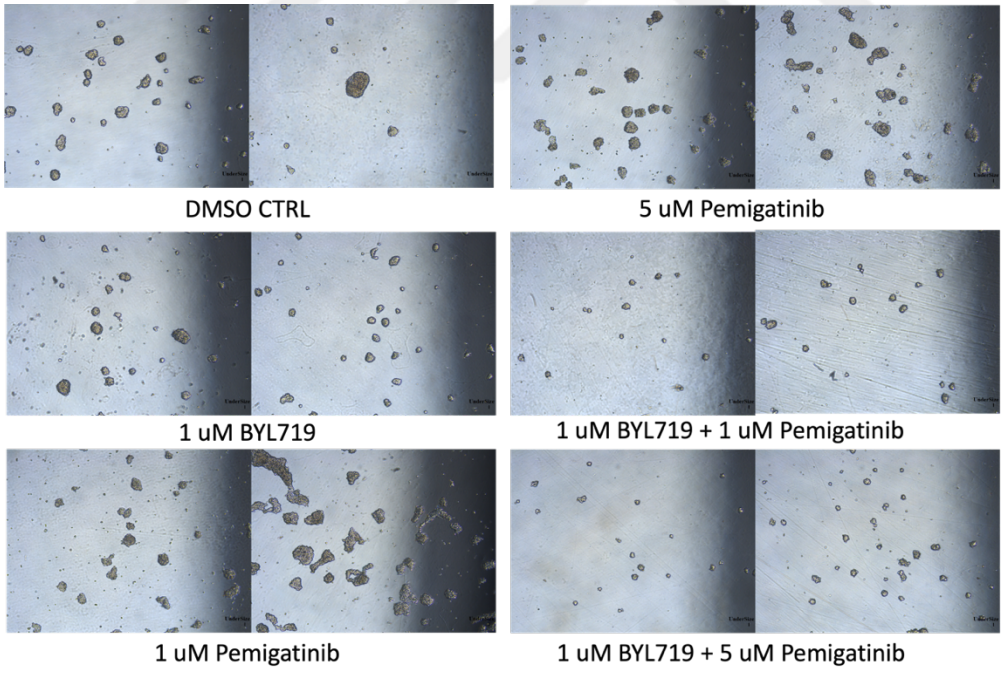

Figure 3.10.3 Microscopy Images of MCF7 BYLR Spheroids Images are acquired with LAS-X Software with Leica DMi8 Microscope. 5x Lens is used along with 10x eyepiece lens, (40x magnification). Cells were cultured in maintanence media with the indicated doses of the inhibitors for 10 days.

We used Arivis Cloud automated image analysis tool to measure the areas of each spheroid arbitrarily. The average area of the spheroids in each different condition was calculated (Figure 3.8.3, Figure 3.8.4). We showed that neither Pemigatinib nor Alpelisib was effective in inhibiting spheroid growth when used as a single treatment. However, when two drugs are combined to treat spheroids, the average spheroid area is decreased at least 2.5-fold for T47D BYLR and 2-fold for MCF7 BYLR compared to the DMSO control. Therefore, we confirmed that the combination of Pemigatinib and Alpelisib is not only effective in inhibiting 2D growth but also has a potency to inhibit 3D growth of T47D BYLR and MCF7 BYLR cells (Figure 3.8.4).

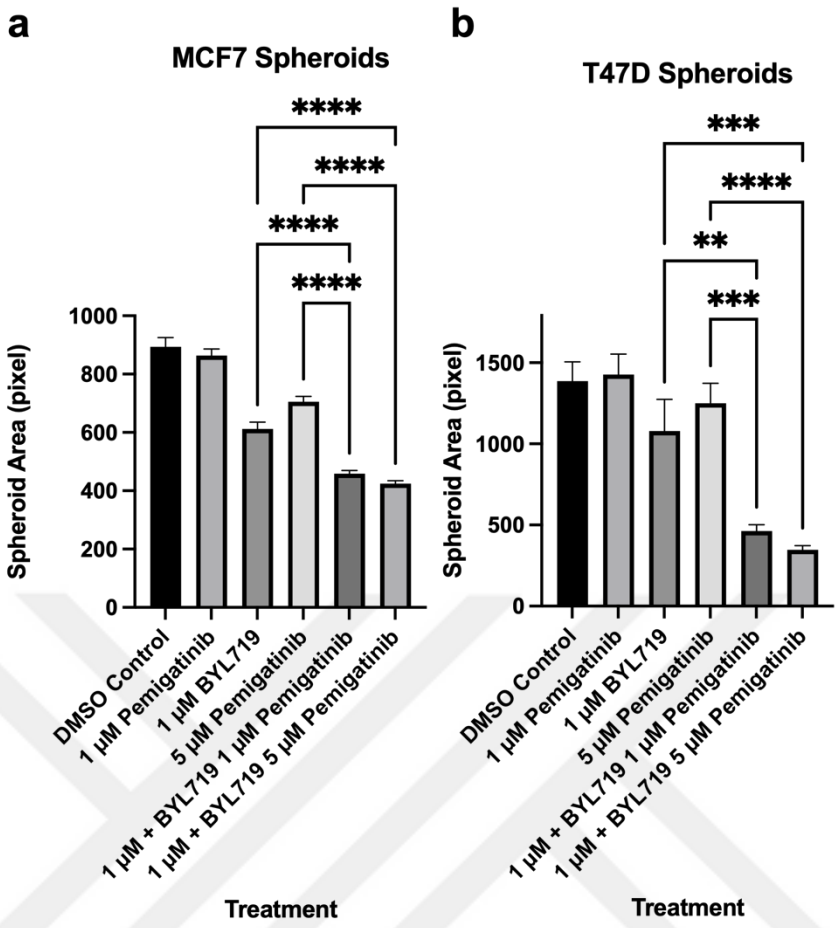

Figure 3.10.4 Spheroid Size Graphs a. T47D BYLR cell line spheroids, b. MCF7 BYLR cell line spheroids. The graphs are generated by GraphPad Prism Software; SEM was used to draw error bars. The spheroid area was shown as pixels. Treated drugs were shown in the x-axis. 2-way ANOVA was used to test significance. P values for ****≤ 0.0001, ***≤ 0.001, **≤ 0.01, *≤ 0.05, ns ≤ 005

3.11 Biochemical Analysis after Combinatory Inhibition Experiments

Since we hypothesised that after acquiring resistance to PIK3CA inhibitor Alpelisib, the cells exploit MAPK and FGFR pathways in order to overcome PI3K pathway inhibition, we wanted to check the protein expression levels of MAPK pathway members, PI3K activation markers after treating with combinatory treatment as well as the single uses of each

inhibitor. We treated T47D cells with 5 μM of Pemigatinib, 1 μM of Alpelisib, the combination of 5 μM of Pemigatinib and 1μM of Alpelisib and the corresponding amount of DMSO for the control. The treatment duration was 6 hours for the T47D BYLR cell line. On the other hand, MCF7 BYLR cells were treated with 5 M of Pemigatinib and 0.75 μM of Alpelisib. The combination of 5 μM of Pemigatinib and 0.75 μM of Alpelisib and the corresponding amount of DMSO for the control and the treatment duration was 24 hours. After the treatments were ended, all the cells were scraped and lysed with urea lysis buffer.

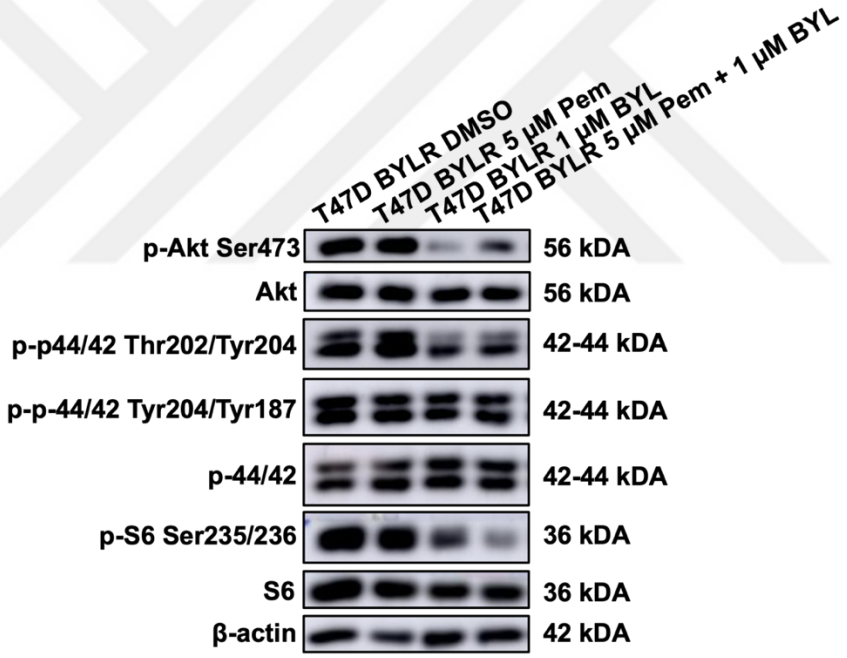

Figure 3.11.1 T47D BYLR Western Blot after Combinatory Treatment 20 μg of protein was loaded into each well and samples were run in 10% gel. Cells were treated with the indicated doses of inhibitors for 6 hours. The β-actin panel was used as the loading control.

In Figure 3.9.1, although we did not observe a further inhibition of phosphorylated p-44/42 (MAPK) with the combination treatment when compared to the single use of Alpelisib in T47D BYLR cell lines, the abundance of the protein is still lower than the DMSO control group. Moreover, the inhibition of Ser235/236 phosphorylated S6 protein, which shows the activation of the mTOR pathway, is more potent when combinatory treatment is used compared to the single use of each drug.

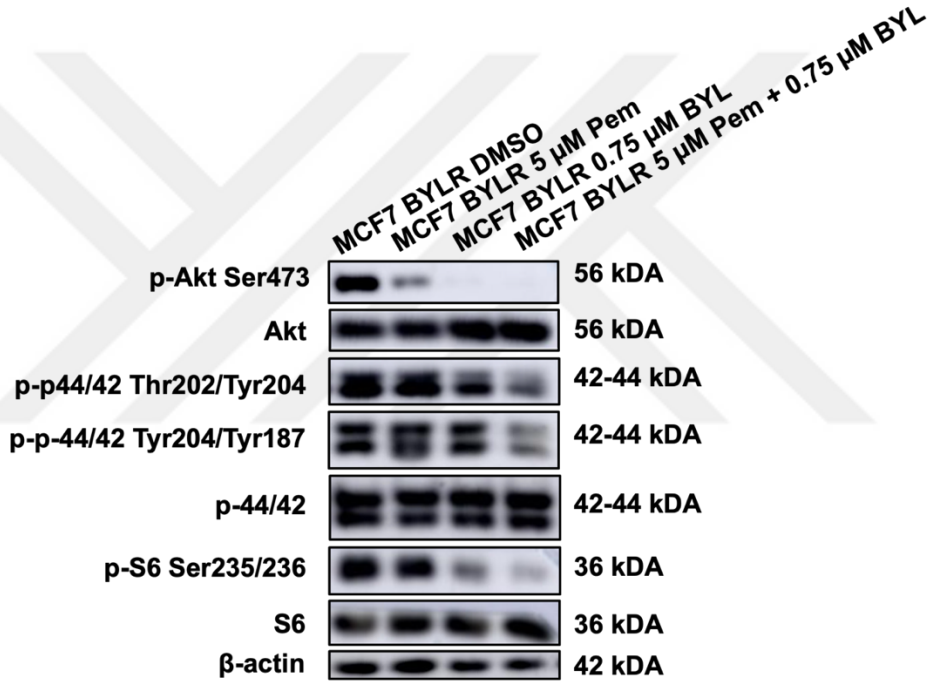

Figure 3.11.2 MCF7 BYLR Western Blot after Combinatory Treatment 20 μg of protein was loaded into each well and samples were run in 10% gel. Cells were treated with the indicated doses of inhibitors for 24 hours. The β-actin panel was used as the loading control.

The dual phosphorylations of MAPK, namely p-p-44/42 Thr202/Tyr204 and p-p-44/42 Tyr202/Tyr87 are required for a fully activated form of MAPK. In Figure 3.9.2, we see a more potent inhibition of dual phosphorylated forms

of MAPK when the Alpelisib-Pemigatinib combination is used compared to the single uses of both inhibitors for MCF7 BYLR cells. We also observed that phosphorylated Akt on Ser473 residue and phosphorylated S6 on Ser235/236 residues, which occur downstream to the mTOR pathway, are also decreased in the MCF7 BYLR cell line in combinatory treatment.

3.12 Expression of FGFR3 in T47D fulvR Cell Line

In order to understand whether the upregulation of the constitutively active form of FGFR3 leads to a alpelisib tolerance in non-resistant cell lines, we first stably transfected T47D fulvR cell lines with TEL-FGFR3. We also stably transfected negative control cells with pBabe Neo, the empty vector. To validate the expression of TEL-FGFR3 in T47D fulvR cells, we performed a Western Blot analysis against FLAG since these constructs include FLAG tags.

The size of FGFR3 is 128.3 kDa, and the size of the FLAG tag with the TEL domain is approximately 16 kDa. Therefore, if FGFR3 is successfully transduced, we expected a band for anti-FLAG at approximately 140 kDa. In Figure 3.9.1, we observed a band exactly where we expected. Therefore, the expression of TEL-FGFR3 was successful in T47D fulvR cell line.

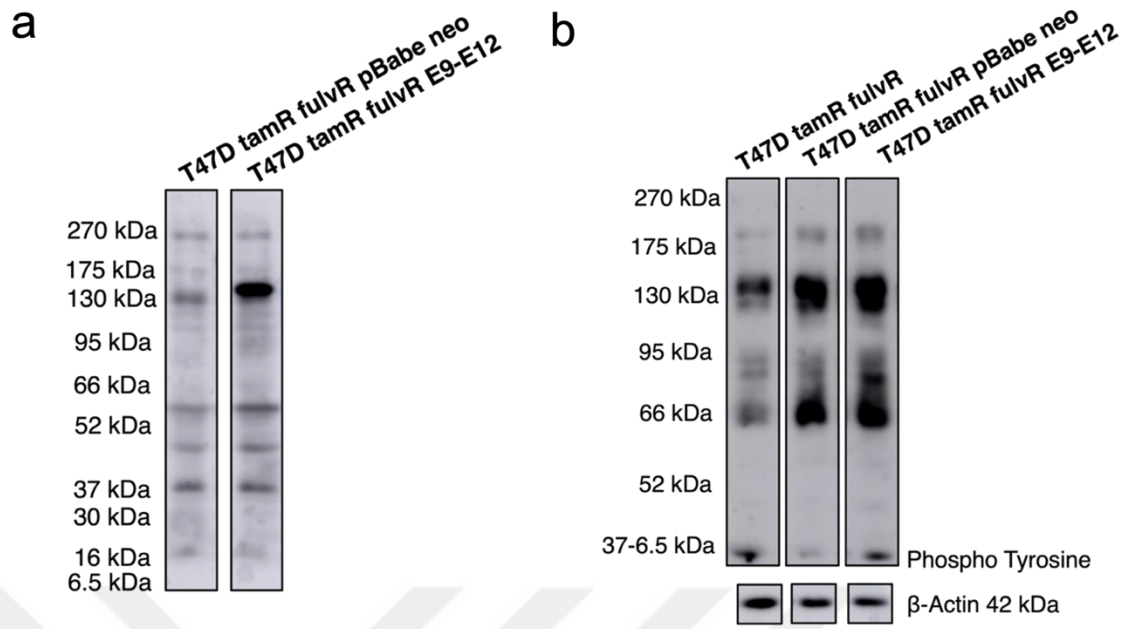

Figure 3.12.1 Immunoblots for FLAG and Phospho Tyrosine a. FLAG immunoblot; 20 μg of protein was loaded into each well and samples were run in 10% gel. b. Phopho-tyrosine immunoblot; 20 μg of protein sample was loaded into each well. Samples were run in 8% resolving gel. β-Actin panel is used as a loading control.

Compared to empty vector and control cells, p-Tyr levels around 70 kDa and 175 kDa are upregulated, implying that FGFR3 protein is functional in this cell line. After validating that FGFR3 is stably expressed and functional, we conducted a dose escalation experiment on T47D fulvR and T47D fulvR, which expresses constitutively active FGFR3 against alpelisib.

3.13 Alpelisib Dose Excalation in FGFR3 Expressing Cell Line

We expected an acquired resistance to Alpelisib in the cells with exogenous expression of FGFR3 since we observed an enrichment and upregulation of the FGFR pathway, especially FGFR3 involvement in signal

transduction in the Alpelisib-resistant cell lines. However, the Alpelisib dose escalation experiment did not give the expected results, as can be seen from the SRB staining in Figure 3.13.1 and the IC50 graph of Alpelisib for two cell lines in Figure 3.13.2

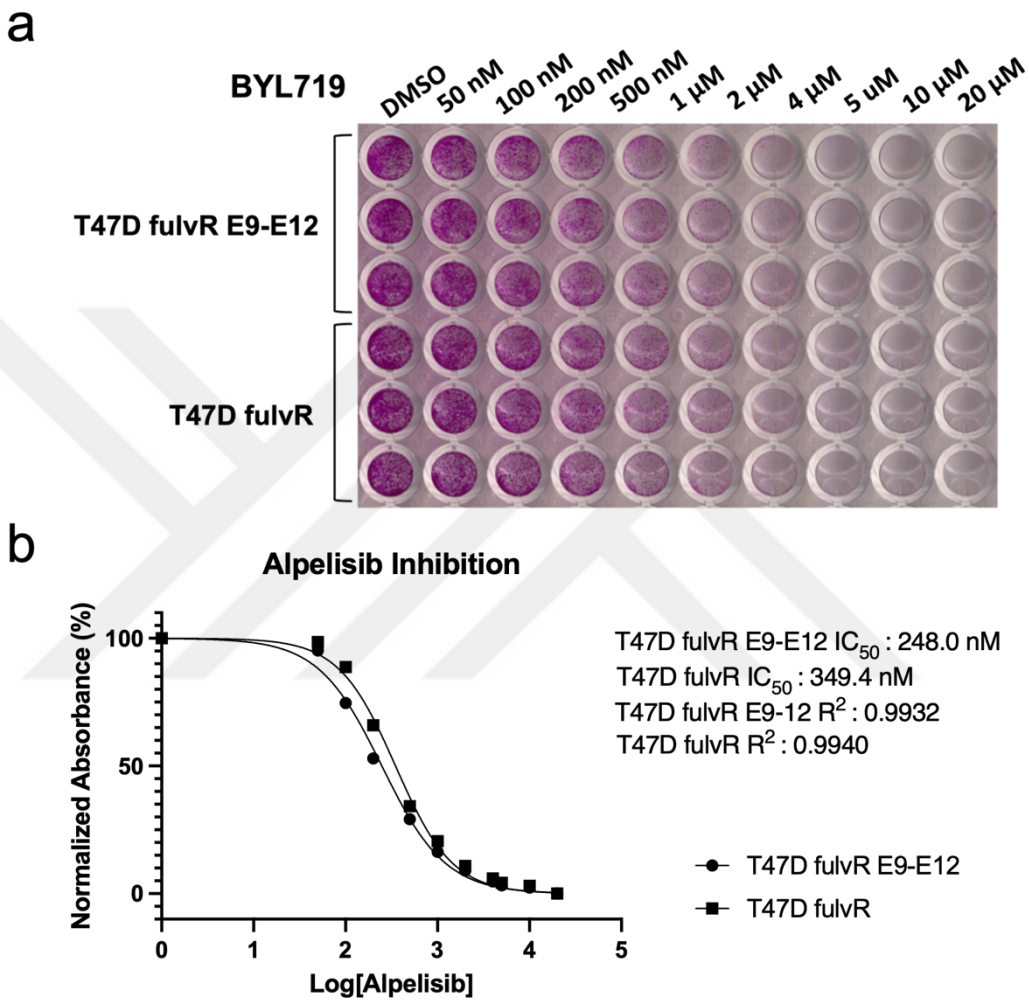

Figure 3.13.1 Cell Viability Assay in FGFR3 expressing T47D fulvR Cell Line with the Control a. SRB staining image. b. Percent Inhibition Graph for Alpelisib. DMSO is used as vehicle. 3000 cells were seeded into each well. Cells were cultured in maintenance media with the indicated doses of inhibitors till the DMSO control group reached 80% confluency. Each dose is treated in triplicates. T47D fulvR E9-E12 (FGFR3 expressing) cell line was represented with square, and T47D fulvR (control) was represented by a circle. SEM was used to draw error bars; however, error bars cannot be seen in this scale since the error rate is too low.

4. DISCUSSION

Cancer is a leading reason for death, and breast cancer is the most prevalent cancer type. Luminal A breast cancer, which is characterised by hormone receptor positivity and HER2 receptor negativity, is the most prevalent subtype, accounting for approximately 50% of all reported breast cancers. PI3K pathway components are commonly mutated in Luminal A breast cancers. Especially, PIK3CA mutations are the most frequently seen mutations in Luminal A breast cancer after p53 mutations (Bader et al.). Therefore, PI3K pathway inhibitors are employed to treat breast tumours characterised by PIK3CA mutations (World Health Organization).

Drug resistance is still a major challenge in cancer therapy. Resistance may be intrinsic or acquired, and resistance may develop as a result of the therapy (Vasan et al.). Therefore, understanding the resistance mechanisms may pave the way to developing more effective and comprehensive alternative therapies. This study focuses on the identification of potent resistance mechanisms to Alpelisib-Fulvestrant therapy.

We first aimed to develop acquired resistance against the Alpelisib-Fulvestrant combination, which has recently been proven successful for breast cancer patients with PIK3CA mutant tumours. By subjecting the resistant cells and their non-resistant controls to comparative transcriptomic analysis, we were able to identify the differentially expressed genes among two cohorts.

MCF7 and T47D cell lines are hormone receptor-positive and HER2-negative breast cancer cellular models. MCF7 carries a PIK3CA E545K

mutation in the helical domain, while T47D carries a PIK3CA H1047R mutation in the kinase domain (Beaver et al., 2013) (Keraite et al., 2020). Moreover, we used tamoxifen-resistant cell lines in our study since we considered that patients eligible to take Alpelisib-Fulvestrant therapy may have already taken hormone therapy. Therefore, our approach is relevant to study resistance mechanisms against Alpelisib-Fulvestrant therapy.

We validated that the cells we use are resistant to tamoxifen compared to the parental cell lines (**Figure 3.1.1**). Then, we started the resistance development process with our strategy, shown in **Figure 3.2.2.** As a result, tamoxifen-resistant MCF7 and T47D cell lines developed acquired resistance against Alpelisib-Fulvestrant compared to their control cohorts (**Figure 3.3.1**). IC_{50} values of Alpelisib-Fulvestrant resistant MCF7 and T47D cell lines increased approximately 3.5 fold for MCF7 and 12 fold for T47D compared to the controls. Due to the selective pressure exerted by the drug, certain tumour cell populations within the collective are naturally selected and can dominate, which leads to the development of acquired resistance (Wright et al.). We hypothesised that the same mechanism could take place against the Alpelisib-Fulvestrant combination, and our primary results validated that these cells are able to gain resistance to this therapy.

We wanted to identify the differentially expressed genes between two cohorts, resistant and non-resistant, via RNA sequencing. Therefore, we isolated total RNA from both cohorts in triplicates and sent the samples to RNA sequencing. We wanted to find a common resistance mechanism against the Alpelisib-Fulvestrant combination in both cell lines, which models

Luminal A breast cancer. Therefore, the common DEGs in MCF7 BYLR and T47D BYLR cell lines are filtered compared to the control cohorts to identify the common significantly downregulated and upregulated genes. We observed 33 commonly upregulated and 28 commonly downregulated genes in MCF7 BYLR and T47D cell lines (**Figure 3.6.1.2)**. These might spot the genes which might be involved in the resistance to the Alpelisib-Fulvestrant combination since they are differentially expressed in both cell lines. We conducted literature research for these genes and *in silico* analyses to detect potential factors responsible for drug resistance.

We wanted to check the differential expression levels of the genes involved in PI3K pathway to identify the changes in transcriptional levels upon acquiring resistance to Alpelisib. We generated the heatmap for PIK3CA, PIK3CB, PIK3CD PTEN, AKT1, MTOR, RICTOR and RAPTOR. Since PIK3CD and RAPTOR levels are not diffrerentially expressed in two cohorts, these genes are not strong candidates for bypassing resistance. In **Figure 3.6.3.1** we observe the downregulation of PTEN and the upregulation of PIK3CB, MTOR and RICTOR in T47D BYLR cell lines compared to the control cohorts. Upon acquiring resistance T47D cell lines downregulated PTEN, the negative regulator of PI3K pathway. Thus, although Alpelisib inhibits p110α, the negative feedback loop is dysregulated due to the downregulation of PTEN, and the pathway remains more active, which leads to drug resistance (Bosch et al.). On the other hand, PIK3CA, PIK3CB, MTOR and RICTOR are upregulated in T47D Alpelisib-resistant cell lines compared to the controls. PIK3CA and PIK3CB are the catalytic subunits of

PI3K and Alpelisib specifically inhibits p110α. Since the cells are continuously cultured with Alpelisib, p110α is inhibited; T47D-resistant cells upregulated the PIK3CA gene to compensate for the inhibition and as a result, cells become resistant to Alpelisib.

PTEN, PIK3CA, PIK3CB, MTOR, RICTOR are upregulated and AKT1 is downregulated in MCF7 BYLR cell lines compared to the control cohorts (**Figure 3.6.3.1**). Likewise, the mechanism in T47D Alpelisib-resistant cell lines, MCF7 Alpelisib-resistant cell lines also upregulated PIK3CA and PIK3CB gene. Inhibition of p110α protein was bypassed by the upregulation of PIK3CA gene. Thus, pathway remains activated which confers resistance to Alpelisib. Upregulation of PIK3CB might show a compensatory mechanism to keep PI3K pathway activated. So, when p110α is inhibited, cells might be trying to activate p110β to bypass Alpelisib inhibition. Upregulation of the other signal transducers of PI3K pathway shows the same mechnanism. However; we observe an opposite trend for AKT1, it is downregulated in Alpelisib resistant cell lines compared to the controls. So we hypothesise that resistance is not taking place through AKT1, and cells still might be sensitive to AKT inhibitors (Wright et al.).

We performed a gene ontology analysis with the differentially expressed genes in Alpelisib-resistant cell lines to determine which pathways are enriched after acquiring resistance against Alpelisib. We used upregulated and downregulated genes at the same time to perform the analysis to understand the collective effect of all DEGs. Pantherdb analysis helped to visualise which terms are enriched in T47D BYLR and MCF7 BYLR

cell lines. In **Figure 3.7.1.1**, it is seen that FGFR and MAPK signalling pathways are enriched, and these terms account for nearly 30% of the all-enriched terms among 400 pathway hits.

It has been shown before that inhibiting the PI3K/AKT/mTOR pathway may trigger the activation of receptor tyrosine kinases (RTKs) such as IGFR-1, EGFR, HER2, and HER3 (O'Reilly et al. and Chakrabarty A., et al.). This activation can, in turn, stimulate downstream pathways, including both the PI3K/AKT/mTOR and Ras/Raf/MEK/ERK pathways, potentially reducing the effectiveness of treatments that target the PI3K/AKT/mTOR pathway (Serra et al.). In our Alpelisib-resistant cells, the same negative feedback mechanism might be taking place and leading to the activation of the MAPK pathway. Moreover, it has been demonstrated that inhibition of PI3K delta isoform can lead to the activation of MAPK and, as a result, lead to drug resistance in chronic lymphocytic leukaemia patients (Okkenhaug 3). Therefore, the isoform-specific inhibition of the PI3K pathway may lead to the activation of the MAPK pathway, which is parallel to the results obtained from our RNASeq experiments. We checked the genes that are involved in enriched pathways and observed that FGF receptors are activating the enriched pathways. Therefore, we hypothesise that PIK3CA inhibition might lead to an FGFR-mediated reactivation of the MAPK pathway, which in turn decreases the effectiveness of the PI3K inhibitor and causes therapeutic resistance.

From Reactome Pathway analysis with DAVID for T47D BYLR cell line **(Figure 3.7.2.1)**, we observed that signalling by receptor tyrosine kinases is

the most enriched term with the highest number of DEGs. As stated above, PI3K inhibition may lead to the activation of RTKs, subsequently decreasing the effectiveness of the PI3K inhibitors. We also observed the enrichment of MAPK family signalling cascades and signalling by NRTKs and VEGF.

Upon activation of VEGFR by VEGF, PLCγ activates second messengers and downstream signalling events, resulting in the activation of MAP2/ERK kinase (MEK). Some members of non-receptor tyrosine kinases (NRTKs), on the other hand, are capable of regulating RAS/RAF/MEK/ERK MAPK and VEGF pathways and are suspected to have a role in the progression of leukaemia. When taken together, enrichment of the pathways in the Alpelisib-resistant T47D cell line might point out a MAPK activation to overcome the PIK3CA inhibition.

MCF7 BYLR Reactome Pathway analysis by DAVID showed that signal transduction is the most significantly enriched term involving the highest number of genes. These genes included many FGF receptors, which show an FGFR-mediated pathway activation. Signalling by receptor tyrosine kinases is also enriched in these cells (**Figure 3.7.2.2**). However, it seems like MAPK activation is also taking place with a different signalling mechanism than T47D BYLR cells. IGF1R signalling cascade, IRS-mediated signalling, and insulin receptor signalling cascade are some of the enriched pathways. IGF receptor is capable of signalling to both MAPK and PI3K cascades through second messengers (Werner et al.). Thus, many enriched pathways point out a regulation of the MAPK pathway, which led us to

conclude that the activation of the MAPK pathway might be responsible for the resistance to Alpelisib.

We also performed a ClueGO analysis to visualise the enriched terms in a network-based manner. This analysis showed the enrichment of similar terms to DAVID analysis as well as providing the relation of the terms to each other (**Figure 3.7.3.1** and **Figure 3.7.3.2**). We also wanted to investigate whether the DEGs in resistant cell lines are interacting with each other. In **Figure 3.7.4.1,** we observed that MAPK members are not only commonly differentially expressed but also have many strong interactions with the other DEGs. Therefore, we think these genes have a common contextual interaction to regulate cellular events.

Since we encountered several enrichments for the activation of MAPK cascade and the genes involved in the enrichments included FGFR members, we hypothesised that to overcome the PIK3K pathway inhibition, MCF7 BYLR and T7D BYLR cells might be alternatively activating the MAPK pathway in an FGFR mediated manner to sustain their survival and growth. Therefore, we expected the upregulation of MAPK pathway proteins and conducted a biochemical analysis with relative antibodies. Our western blotting analysis (**Figure 3.8.1**) showed that total MAPK levels are increased in both resistant cell lines compared to their control cohorts, 2.8-fold in MCF7 BYLR and 1.7-fold in T47D BYLR cells. The double and single phosphorylated forms of MAPK (p-p-44/42 Tyr202 and p-p44/42 Tyr202/204) also significantly upregulated in resistant cell lines. Phosphorylated forms of the MAPK are required for the pathway activation. Therefore, MAPK

signalling seems activated in resistant cell lines compared to their controls. Thus, we confirmed our hypothesis that resistant cell lines hyperactivated the MAPK signalling cascade to overcome PI3K inhibition.

Phospho-tyrosine levels can be predictive of the activation of FGFRs since they undergo autophosphorylation on many tyrosine residues when activated (Pantani et al., 2016). Furthermore, the activation of FGFRs leads to the activation of the MAPK pathway. Therefore, we also conducted a western blot analysis for photo-tyrosine substrates to assess the activation of FGFRs and the MAPK pathway indirectly. In **Figure 3.8.2,** we observed an upregulation pattern in tyrosine phosphorylation in resistant cell lines compared to the controls. There seems to be a significant upregulation, especially around ~170 kDa, ~130 kDa and ~60 kDa proteins. This pattern is also found to be related with poor prognosis in lung cancer (Nishimura et al., 1996). Thus, we can say that the upregulation of tyrosine phosphorylation may reflect the activation of FGFRs and MAPK pathway, which is predicted to be activated in our cells due to acquired resistance against the Alpelisib-Fulvestrant combination.

After validating our results with immunoblot experiments that the MAPK signalling pathway is activated in resistant cell lines, we wanted to use an FGFR inhibitor since we hypothesize that the activation of the MAPK pathway is taking place via FGFRs. Pemigatinib is an FGFR inhibitor, and it was recently approved by the FDA for the treatment of cholangiocarcinoma (Patel et al., 2023). Since the PI3K pathway is overactivated due to the acquired resistance in BYLR cell lines, we used Pemigatinib combined with

alpelisib to inhibit the PI3K pathway to its basal level. Dose escalation of Pemigatinib on MCF7 BYLR and T47D BYLR cell lines showed no significant inhibition (**Figure 3.9.1, Figure 3.9.2** and **Figure 3.9.3**). However, when alpelisib and Pemigatinib are combined, cell viability significantly dropped to 25% and 40% for MCF7 BYLR and T47D BYLR, respectively. When CI values were assessed, we observed a good synergy between alpelisib and Pemigatinib (**Table 3.9.1**). Therefore, we suggest that the use of FGFR inhibitor Pemigatinib in combination with alpelisib might be an alternative approach in breast cancer tumours which are characterised to be resistant to Alpelisib-Fulvestrant therapy. We further validated our approach by performing 3D spheroid growth assays with Pemigatinib and alpelisib combination treatments. We observed that the single use of both inhibitors was ineffective in preventing the initiation and the growth of spheroids (**Figure 3.10.2, Figure 3.10.3** and **Figure 3.10.4**). However, the combinatory use of Pemigatinib along with alpelisib significantly decreased the spheroid area, reflecting the success of the combination in inhibiting the initiation and growth of spheroids.

After validating that the combinatory use of Alpelisib+Pemigatinib is more potent than the single use of each drug to inhibit 2D and 3D growth, we wanted to perform a biochemical analysis to see if the inhibitory effect of the treatment combination is also exerting its effect at protein expression level. In **Figure 3.11.1**, combination treatment does not seem more potent than the single use of alpelisib; yet, p-p44/42 Thr202/Tyr204 level is still lower than the control cells. We suspect that the MAPK activation might be through the

p38-MAPK module (Roux et al.) in T47D BYLR cells rather than ERK1/2; therefore, we are not able to see the downregulation of phosphorylated p-44/42. However, we see the downregulation of p-S6 on Ser235/236 residue, which is activated downstream to PI3K and MAPK cascades.

Phosphorylated S6 is involved in cell proliferation and growth events, so the further downregulation of this protein shows the potency of combination treatment over the single use of each drug. We may conclude that, although the combination does not further downregulate ERK1/2 activated forms, the cells are sensitive to the inhibition by the Alpelisib+Pemigatinib combination treatment implies that MAPK cascade activation might be through another MAPK family, such as p38 and inhibition by combination treatment works through another pathway.

In MCF7 BYLR cell lines, we observed a more potent downregulation of the dual phosphorylated forms of p-44/42, which shows the full activation of p-44/42 protein when combination treatment is used versus the single uses of Pemigatinib and Alpelisib (**Figure 3.11.2**). Phophorylations of Akt and S6 are checked to assess the proliferative rate of the cells (Meyuhas). It is observed that p-Akt Ser473 and p-S6 Ser23/236 levels are significantly decreased; p-S6 is even less abundant in combined treatment compared to the single uses of each treatment. So, when cells are treated with Alpelisib-Pemigatinib combination, the proliferation and growth of the cells are decreased. Although the cells are resistant to Alpelisib, both cell lines are responsive to Alpelisib in terms of Akt expression levels. However, since we observed the downregulation of AKT1 gene in **Figure 3.6.3.1** and

hypothesized that resistance is taking place mainly through PIK3CA and the other upregulated genes rather than AKT1, the resistant cells are still sensitive to Akt inhibition. Conclusively, the combination treatment is more effective in inhibiting the MAPK pathway in MCF7 cell lines when compared to the Alpelisib and Pemigatinib treatments. The inhibitory effect of the combination treatment is proven to be decreasing the MAPK related protein expression levels, especially dual phophorylations of Erk1/2. This implies that the FGFR-mediated MAPK activation through acquiring resistance to Alpelisib can be inhibited with FGFR inhibitor Pemigatinib and PIK3CA inhibitor Alpelisib when cells acquire resistance to Alpelisib.

We have proven that the FGFR-mediated activation of the MAPK cascade leads to resistance against the PIK3CA inhibitor Alpelisib. Therefore, we wanted to perform a reverse approach to our findings, expressing the constitutively active FGFRs in non-resistant cell lines to determine if it leads to resistance to Alpelisib. In **Figure 3.12.1** it is seen that the FLAG-tagged TEL-FGFR3 is successfully expressed in T47D fulvR cell lines. Phospho-tyrosine blot also showed an upregulation of tyrosine phosphorylated proteins compared to the backbone transfected cell line (**Figure 3.12.2**). Therefore, we concluded that TEL-FGFR3 is exogenously expressed in T47D fulvR cells. Then, we performed a dose escalation experiment for Alpelisib to find out if the FGFR3 overexpressing cells gained resistance to the treatment. However, we did not observe a significant sensitivity difference between T47D fulvR cells and the T47D cells transfected with TEL-FGFR3 (**Figure 3.13.1** and **Figure 3.13.2**).

One of the potential explanations might be the involvement of other FGFR family members in activating the MAPK pathway to confer resistance. It is plausible that the MAPK cascade activation might be taking place through FGFR1 or FGFR2 rather than FGFR3. Additionally, these receptors might be working coordinately to mediate Alpelisib resistance, and thus, overexpressing FGFR3 might be insufficient to mimic naturally acquired resistance. This suggests that the resistance to Alpelisib is not solely dependent on FGFR activation but is intricately linked to the specific FGFR isoforms involved or their interaction. This underscores the complexity of receptor-mediated signalling in therapeutic resistance.

5. CONCLUSION AND FUTURE PERSPECTIVES

In this study, we proved that Luminal A breast cancer cell models MCF7 and T47D are capable of acquiring resistance against Fulvestrant-Alpelisib treatment. One of the resistance mechanisms involved in this process might be via activation of the MAPK pathway. Our results indicate an FGFR mediated activation of MAPK pathway to overcome the PIK3K inhibiton to find an alternative signalling pathway to sustain cell viability and growth. Therefore, cells become resistant to the Alpelisib-Fulvestrant combination and continue to grow thanks to the activation of the MAPK cascade. In case PIK3CA mutant Luminal A breast cancer patients develop resistance against Alpelisib therapy, FGFR inhibitor Pemigatinib can be used in combination with alpelisib as an alternative approach.

A detailed biochemical analysis can be conducted by purchasing FGFR-specific anticores. Thus, FGFR-mediated activation of the MAPK pathway can be directly observed in Alpelisib-resistant MCF7 and T47D cell lines. The key genes that are involved in FGFR-mediated MAPK cascade activation can be studied by overexpressing the downregulated genes or knocking down the upregulated genes in resistant cell lines to check if they sensitise the cells back to Alpelisib-Fulvestrant therapy. Pemigatinib and Alpelisib combination can also be used in mouse MCF7 BYLR and T47D BYLR xenografts in order to see if the efficacy of the combination is also relevant for in vivo studies as well as assess the toxicity of the combinatory use.

BIBLIOGRAPHY

André, F., et al. “Alpelisib plus Fulvestrant for PIK3CA-mutated, Hormone Receptor-positive, Human Epidermal Growth Factor Receptor-2-negative Advanced Breast Cancer: Final Overall Survival Results from SOLAR-1.” *Annals of Oncology: Official Journal of the European Society for Medical Oncology*, vol. 32, no. 2, 2021, pp. 208-217. doi:10.1016/j.annonc.2020.11.011.

Bader, Andreas G et al. “Cancer-specific mutations in PIK3CA are oncogenic in vivo.” *Proceedings of the National Academy of Sciences of the United States of America* vol. 103,5 (2006): 1475-9. doi:10.1073/pnas.0510857103

Balko, Justin M et al. “Activation of MAPK pathways due to DUSP4 loss promotes cancer stem cell-like phenotypes in basal-like breast cancer.” *Cancer research* vol. 73,20 (2013): 6346-58. doi:10.1158/0008-5472.CAN-13-1385

Beaver, Julia A et al. “PIK3CA and AKT1 mutations have distinct effects on sensitivity to targeted pathway inhibitors in an isogenic luminal breast cancer model system.” *Clinical cancer research : an official journal of the American Association for Cancer Research* vol. 19,19 (2013): 5413-22. doi:10.1158/1078-0432.CCR-13-0884

Bindea, Gabriela et al. “ClueGO: a Cytoscape plug-in to decipher functionally grouped gene ontology and pathway annotation networks.” *Bioinformatics (Oxford, England)* vol. 25,8 (2009): 1091-3. doi:10.1093/bioinformatics/btp101

Bosch, Ana, et al. “PI3K Inhibition Results in Enhanced Estrogen Receptor Function and Dependence in Hormone Receptor-Positive Breast Cancer.” *Science Translational Medicine*, vol. 7, no. 283, 2015, pp. 283ra51. doi:10.1126/scitranslmed.aaa4442.

Braicu, Cornelia et al. “A Comprehensive Review on MAPK: A Promising Therapeutic Target in Cancer.” *Cancers* vol. 11,10 1618. 22 Oct. 2019, doi:10.3390/cancers11101618

Cargnello, Marie, and Philippe P Roux. “Activation and function of the MAPKs and their substrates, the MAPK-activated protein kinases.” *Microbiology and molecular biology reviews : MMBR* vol. 75,1 (2011): 50-83. doi:10.1128/MMBR.00031-10

Carlson, Robert W. “The History and Mechanism of Action of Fulvestrant.” *Clinical Breast Cancer*, vol. 6, Suppl 1, 2005, pp. S5-8. doi:10.3816/cbc.2005.s.008.

Di Nicolantonio, Federica, et al. “Deregulation of the PI3K and KRAS Signaling Pathways in Human Cancer Cells Determines Their Response to Everolimus.” *The Journal of Clinical Investigation*, vol. 120, no. 8, 2010, pp. 2858-2866. doi:10.1172/JCI37539.

Chakrabarty, A., et al. "Feedback Upregulation of HER3 (ErbB3) Expression and Activity Attenuates Antitumor Effect of PI3K Inhibitors." *Proceedings of the National Academy of Sciences of the United States of America*, vol. 109, 2012, pp. 2718–2723.

Fan, Meiyun et al. “Characterization of molecular and structural determinants of selective estrogen receptor downregulators.” *Breast cancer research and treatment* vol. 103,1 (2007): 37-44. doi:10.1007/s10549-006-9353-2

Fekete, J., and B. Gyorffy. “ROCplot.org: Validating Predictive Biomarkers of Chemotherapy/Hormonal Therapy/Anti-HER2 Therapy Using Transcriptomic Data of 3,104 Breast Cancer Patients.” *International Journal of Cancer*, vol. 145, no. 11, 2019, pp. 3140-3151. doi:10.1002/ijc.32369.

Ferraro, Bernadette et al. “EGR1 predicts PTEN and survival in patients with non-small-cell lung cancer.” *Journal of clinical oncology : official journal of the American Society of Clinical Oncology* vol. 23,9 (2005): 1921-6. doi:10.1200/JCO.2005.08.127

Galstyan, Arpine, et al. “Modulation of the PI3K/mTOR Pathways.” *Cancer Sensitizing Agents for Chemotherapy, Improving the Therapeutic Ratio in Head and Neck Cancer*, edited by Randall J. Kimple, vol. 6, Academic Press, 2020, pp. 89-105. ScienceDirect, https://doi.org/10.1016/B978-0-12-817868-3.00005-6.

Goetz, Regina, and Moosa Mohammadi. “Exploring mechanisms of FGF signalling through the lens of structural biology.” *Nature reviews. Molecular cell biology* vol. 14,3 (2013): 166-80. doi:10.1038/nrm3528

Gyorffy, B. “Integrated Analysis of Public Datasets for the Discovery and Validation of Survival-Associated Genes in Solid Tumors.” *The Innovation*, 2024. https://pubmed.ncbi.nlm.nih.gov/38706955/.

Gyorffy, B. “Transcriptome-level Discovery of Survival-Associated Biomarkers and Therapy Targets in Non-small-cell Lung Cancer.” *British Journal of Pharmacology*, 2024. https://pubmed.ncbi.nlm.nih.gov/37783508/.

Harbeck, Nadia et al. “Breast cancer.” *Nature reviews. Disease primers* vol. 5,1 66. 23 Sep. 2019, doi:10.1038/s41572-019-0111-2

Huang, Da Wei et al. “Systematic and integrative analysis of large gene lists using DAVID bioinformatics resources.” *Nature protocols* vol. 4,1 (2009): 44-57. doi:10.1038/nprot.2008.211

Keraite, I., et al. "PIK3CA Mutation Enrichment and Quantitation from Blood and Tissue." Scientific Reports, vol. 10, no. 1, 2020, p. 17082. https://doi.org/10.1038/s41598-020-74086-w.

Lee, Eung-Ryoung et al. “Interplay between PI3K/Akt and MAPK signaling pathways in DNA-damaging drug-induced apoptosis.” *Biochimica et biophysica acta* vol. 1763,9 (2006): 958-68. doi:10.1016/j.bbamcr.2006.06.006

Ligresti, Giovanni, et al. “PIK3CA Mutations in Human Solid Tumors: Role in Sensitivity to Various Therapeutic Approaches.” *Cell Cycle*, vol. 8, no. 9, 2009, pp. 1352-1358. doi:10.4161/cc.8.9.8255.

Mendoza, Michelle C., et al. “The Ras-ERK and PI3K-mTOR Pathways: Cross-talk and Compensation.” *Trends in Biochemical Sciences*, vol. 36, no. 6, 2011, pp. 320-328. doi:10.1016/j.tibs.2011.03.006.

Meyuhas, Oded. “Ribosomal Protein S6 Phosphorylation: Four Decades of Research.” *International review of cell and molecular biology* vol. 320 (2015): 41-73. doi:10.1016/bs.ircmb.2015.07.006

Movérare-Skrtic, Sofia et al. “The estrogen receptor antagonist ICI 182,780 can act both as an agonist and an inverse agonist when estrogen receptor α AF-2 is modified.” *Proceedings of the National Academy of Sciences of the United States of America* vol. 111,3 (2014): 1180-5. doi:10.1073/pnas.1322910111

Narayan, Preeti, et al. “FDA Approval Summary: Alpelisib Plus Fulvestrant for Patients with HR-positive, HER2-negative, PIK3CA-mutated, Advanced or Metastatic Breast Cancer.” *Clinical Cancer Research: An Official Journal of the American Association for Cancer Research*, vol. 27, no. 7, 2021, pp. 1842-1849. doi:10.1158/1078-0432.CCR-20-3652.

Nathan, Mark R., and Peter Schmid. “A Review of Fulvestrant in Breast Cancer.” *Oncology and Therapy*, vol. 5, no. 1, 2017, pp. 17-29. doi:10.1007/s40487-017-0046-2.

National Center for Biotechnology Information. "PubChem Compound Summary for CID56649450,

“Alpelisib" *PubChem*, https://pubchem.ncbi.nlm.nih.gov/compound/Alpelisib . Accessed 7 August, 2024.

Nishimura, M et al. “Tyrosine phosphorylation of 100-130 kDa proteins in lung cancer correlates with poor prognosis.” *British journal of cancer* vol. 74,5 (1996): 780-7. doi:10.1038/bjc.1996.436

Okkenhaug, Klaus. "How to Resist PI3Kδ Inhibition: Activate MAPK!" *Blood*, vol. 138, no. 1, 2021, pp. 3–4, https://doi.org/10.1182/blood.2021011365.

O'Reilly, K. E., et al. "mTOR Inhibition Induces Upstream Receptor Tyrosine Kinase Signaling and Activates Akt." *Cancer Research*, vol. 66, 2006, pp. 1500–1508.

Patani, Harshnira et al. “Landscape of activating cancer mutations in FGFR kinases and their differential responses to inhibitors in clinical use.” *Oncotarget* vol. 7,17 (2016): 24252-68. doi:10.18632/oncotarget.8132

Patel, Timil H et al. “FDA Approval Summary: Pemigatinib for Previously Treated, Unresectable Locally Advanced or Metastatic Cholangiocarcinoma with FGFR2 Fusion or Other Rearrangement.” *Clinical cancer research : an official journal of the American Association for Cancer Research* vol. 29,5 (2023): 838-842. doi:10.1158/1078-0432.CCR-22-2036

Reinhardt, Kristin, et al. “PIK3CA-mutations in Breast Cancer.” *Breast Cancer Research and Treatment*, vol. 196, no. 3, 2022, pp. 483-493. doi:10.1007/s10549-022-06637-w.

Roux, Philippe P, and John Blenis. “ERK and p38 MAPK-activated protein kinases: a family of protein kinases with diverse biological functions.” *Microbiology and molecular biology reviews : MMBR*vol. 68,2 (2004): 320-44. doi:10.1128/MMBR.68.2.320-344.2004

Samuels, Yardena, and Todd Waldman. “Oncogenic mutations of PIK3CA in human cancers.” *Current topics in microbiology and immunology* vol. 347 (2010): 21-41. doi:10.1007/82_2010_68

Santen, Richard J., et al. “The Role of Mitogen-activated Protein (MAP) Kinase in Breast Cancer.” *The Journal of Steroid Biochemistry and Molecular Biology*, vol. 80, no. 2, 2002, pp. 239-256. doi:10.1016/s0960-0760(01)00189-3.

Serra, Valentino, et al. "PI3K Inhibition Results in Enhanced HER Signaling and Acquired ERK Dependency in HER2-Overexpressing Breast Cancer." *Oncogene*, vol. 30, 2011, pp. 2547-2557.

Sherman, Brad T et al. “DAVID: a web server for functional enrichment analysis and functional annotation of gene lists (2021 update).” *Nucleic acids research* vol. 50,W1 (2022): W216-W221. doi:10.1093/nar/gkac194

Siegel, Rebecca L et al. “Cancer statistics, 2024.” *CA: a cancer journal for clinicians* vol. 74,1 (2024): 12-49. doi:10.3322/caac.21820

Tang D, Chen M, Huang X, Zhang G, Zeng L, Zhang G, Wu S, Wang Y. SRplot: A free online platform for data visualization and graphing. PLoS One. 2023 Nov 9;18(11):e0294236. doi: 10.1371/journal.pone.0294236. PMID: 37943830.

Toska, Eneda, et al. “PI3K Inhibition Activates SGK1 via a Feedback Loop to Promote Chromatin-Based Regulation of ER-Dependent Gene Expression.” *Cell Reports*, vol. 27, no. 1, 2019, pp. 294-306.e5. doi:10.1016/j.celrep.2019.02.111.

Toska, Eneda, et al. “PI3K Pathway Regulates ER-dependent Transcription in Breast Cancer Through the Epigenetic Regulator KMT2D.” *Science*, vol. 355, no. 6331, 2017, pp. 1324-1330. doi:10.1126/science.aah6893.

Vaish, Vivek et al. “NSAIDs may regulate EGR-1-mediated induction of reactive oxygen species and non-steroidal anti-inflammatory drug-induced gene (NAG)-1 to initiate intrinsic pathway of apoptosis for the chemoprevention of colorectal cancer.” *Molecular and cellular biochemistry* vol. 378,1-2 (2013): 47-64. doi:10.1007/s11010-013-1593-y

Xie, Yucheng, Ning Su, Jing Yang, et al. "FGF/FGFR Signaling in Health and Disease." *Signal Transduction and Targeted Therapy*, vol. 5, no. 1, 2020, article 181, https://doi.org/10.1038/s41392-020-00222-7.

Vasan, N., Baselga, J., and Hyman, D.M. "A View on Drug Resistance in Cancer." Nature, vol. 575, 2019, pp. 299-309, https://doi.org/10.1038/s41586-019-1730-1.

Wang, Bin et al. “The Role of the Transcription Factor EGR1 in Cancer.” *Frontiers in oncology* vol. 11 642547. 24 Mar. 2021, doi:10.3389/fonc.2021.642547

Wang, Ying et al. “The adaptor protein CARD9, from fungal immunity to tumorigenesis.” *American journal of cancer research* vol. 10,8 2203-2225. 1 Aug. 2020

Ward, A et al. “Re-expression of microRNA-375 reverses both tamoxifen resistance and accompanying EMT-like properties in breast cancer.” *Oncogene* vol. 32,9 (2013): 1173-82. doi:10.1038/onc.2012.128

Werner, Haim. “The IGF1 Signaling Pathway: From Basic Concepts to Therapeutic Opportunities.” *International journal of molecular sciences* vol. 24,19 14882. 4 Oct. 2023, doi:10.3390/ijms241914882

World Health Organization. "Breast Cancer." World Health Organization, 13 Mar. 2024, www.who.int/news-room/fact-sheets/detail/breast-cancer. Accessed July 2024.

Wright, Sarah Christine Elisabeth, et al. “Mechanisms of Resistance to PI3K Inhibitors in Cancer: Adaptive Responses, Drug Tolerance and Cellular Plasticity.” *Cancers*, vol. 13, no. 7, 2021, p. 1538. doi:10.3390/cancers13071538.

Yersal, Ozlem, and Sabri Barutca. “Biological subtypes of breast cancer: Prognostic and therapeutic implications.” *World journal of clinical oncology* vol. 5,3 (2014): 412-24. doi:10.5306/wjco.v5.i3.412

Zahreddine, Hiba, and Katherine Borden. “Mechanisms and Insights into Drug Resistance in Cancer.” *Frontiers in Pharmacology*, vol. 4, 2013. doi:10.3389/fphar.2013.00028.

Zhang, W., and H. Liu. "MAPK Signal Pathways in the Regulation of Cell Proliferation in Mammalian Cells." *Cell Research*, vol. 12, no. 1, 2002, pp. 9–18, https://doi.org/10.1038/sj.cr.7290105.